https://doi.org/10.5194/egusphere-2026-4862
Preprint. Discussion started: 19 August 2026


# Internal-tide nutrient supply to the euphotic layer: vertical advection versus turbulent diffusion off the Amazon shelf from glider observations

Amine M'hamdi[1,2 3], Ariane Koch-Larrouy[3], Anthony Bosse[4], Isabelle Dadou[1], Vincent Vantrepotte[5], Alex Costa da Silva[2]

[1]LEGOS, Université de Toulouse, CNRS, OMP, IRD, Toulouse, France
[2]Departamento de Oceanografia, Universidade Federal de Pernambuco (DOCEAN/UFPE), Recife, Brazil
[3]CECI CNRS/Cerfacs/IRD, Université de Toulouse, Toulouse, France
[4]Mediterranean Institute of Oceanography, OSU Institut Pytheas, Aix Marseille University, Université de Toulon, CNRS, IRD, Marseille, France
[5]Univ. Littoral Côte d'Opale, CNRS, Univ. Lille, IRD, UMR 8187– LOG– Laboratoire d'Océanologie et de Géosciences, 62930 Wimereux, France

*Correspondence to*: Amine M'hamdi (abn.mhamdi@gmail.com)

**Abstract.** Tropical oligotrophic surface waters are typically nutrient-limited, and internal tides have been proposed as a key mechanism supplying nutrients to the euphotic zone through two complementary physical pathways: vertical advection and turbulent mixing. However, separating and quantifying these two pathways from in situ observations, and assessing their respective ecosystem implications, remains challenging. Unlike previous studies, which have generally investigated these mechanisms separately, this study directly compares their respective contributions within a common observational framework. Here, autonomous glider observations collected during the AMAZOMIX campaign off the Amazon shelf were used to reconstruct nutrient profiles using CANYON-B neural network, identify internal-tide-driven isopycnal and nutrient-associated vertical displacements, and independently estimate turbulent dissipation rates validated against microstructure profiler (VMP) measurements. Vertical nutrient profiles revealed contrasting nutrient limitation regimes, with a nitrate deficit in the upper layer and a silicate deficit at depth.Our results demonstrate that internal-tide-induced vertical advection dominates the mean nutrient enrichment at the base of the euphotic layer ($F_{ADV}$ = 2.3 ± 0.5 mmol $NO_3$ $m^{-2}$ $d^{-1}$ and 0.4 ± 0.1 mmol Si $m^{-2}$ $d^{-1}$), whereas turbulent diffusion provides smaller mean fluxes ($F_{DIFF}$ = 1.07 mmol $NO_3$ $m^{-2}$ $d^{-1}$ and 0.14 mmol Si $m^{-2}$ $d^{-1}$) but remains essential because it represents an irreversible transport pathway and can dominate during episodic high-energy mixing events. Together, these processes modify not only nutrient availability but also nutrient stoichiometry, highlighting internal tides as an important regulator of ecosystem functioning in the western tropical Atlantic. These results suggest that internal tides act both as a nutrient-supply mechanism and as a potential community-structuring process, with implications for nitrate–silicate-dependent phytoplankton groups at the base of the euphotic layer.

https://doi.org/10.5194/egusphere-2026-4862
Preprint. Discussion started: 19 August 2026


## 1 Introduction

Tropical oligotrophic surface waters are generally characterized by low nutrient concentrations and are often limited by the vertical supply of nutrients to the euphotic layer, particularly nitrate (Moore et al., 2013). In these regions, physical processes that enhance the upward transport of nutrients exert a strong control on primary production, phytoplankton biomass, and biogeochemical cycling (Li et al., 2018; Lucas et al., 2011; Tuerena et al., 2019). Understanding how these physical processes regulate nutrient supply remains a major challenge for predicting ecosystem functioning in stratified tropical oceans.

Internal tides are ubiquitous throughout the global ocean and represent a key pathway through which tides can influence upper-ocean stratification, mixing, and ecosystem functioning (Waterhouse et al., 2014; Kunze, 2017; Koch-Larrouy et al., 2010; Assene et al., 2024). Internal tides are generated when the barotropic tide interacts with steep topography, such as shelf breaks, ridges, and seamounts, converting barotropic tidal energy into baroclinic waves that propagate along density interfaces (Baines, 1982; Garrett and Kunze, 2007; Waterhouse et al., 2014). As internal tides propagate away from their generation sites, they may locally enhance shear, turbulence, and vertical mixing, particularly during spring tides periods (Sharples et al., 2007; Bourgault et al., 2011; Villamaña et al., 2017).

Internal tides can affect nutrient supply through at least two distinct mechanisms. First, their vertical displacements can advect isopycnals and nutrient gradients, thereby modifying the nutrient conditions experienced by phytoplankton near the pycnocline and at the base of the euphotic layer (Lande and Yentsch, 1988; Holloway and Denman, 1989; Evans et al., 2008; Garwood et al., 2020; Jacobsen et al., 2023). Second, the dissipation of internal tides can enhance diapycnal turbulent mixing, generating irreversible diffusive nutrient fluxes across the nutricline and into the euphotic layer (Althaus et al., 2003; Sharples et al., 2007; Sharples et al., 2009; Lucas et al., 2011; Tuerena et al., 2019).

However, the relative roles of vertical diffusion and internal-tide-driven advection in supplying nutrients remain poorly constrained. Identifying the dominant mechanism is essential for understanding how internal tides regulate ecosystem dynamics. This distinction is critical because vertical advection and turbulent diffusion have different ecosystem implications. Indeed advection redistributes existing gradients and can generate transient enrichment and new production in the euphotic layer, whereas diffusion represents an irreversible nutrient flux across density surfaces that can also sustain new production (Ma et al 2023, M'hamdi et al 2025,Sharples et al., 2009; Lucas et al., 2011; Tuerena et al., 2019). A major challenge is therefore to quantify these two pathways independently and to assess whether internal tides modulate nutrient distributions or supply limiting nutrients to phytoplankton communities (Villamaña et al., 2017; Tuerena et al., 2019).

The Amazon shelf break provides a relevant natural laboratory to address this question. This region has long been recognized as a hotspot of internal-tide generation, where strong barotropic tides interact with the continental slope and generate energetic baroclinic motions (Baines, 1982; Ivanov et al., 1990; Brandt et al., 2002; Vlasenko et al., 2005; Magalhaes et al., 2016). More recent studies have confirmed that the Amazon shelf and adjacent oceanic region are characterized by intense internal-tide activity, nonlinear internal waves, and interactions with large-scale and mesoscale

https://doi.org/10.5194/egusphere-2026-4862
Preprint. Discussion started: 19 August 2026


circulation features (Tchilibou et al., 2022; de Macedo et al., 2023; Assene et al., 2024; Goret et al., 2026). In particular, glider observations collected off the Amazon shelf during the AMAZOMIX campaign (September 2021) revealed a region strongly influenced by interactions between internal tides, large-scale currents, and mesoscale structures, with internal-tide signatures identified from satellite observations of internal solitary waves, spring–neap variability, semidiurnal M2 spectral energy, and vertical oscillations of isopycnals (M'hamdi et al., 2025).

While the physical generation and propagation of internal tides off the Amazon shelf have been increasingly documented (Magalhaes et al., 2016; Tchilibou et al., 2022; Kouogang et al., 2025; Kouogang et al., 2026; Goret et al., 2026), their biogeochemical and ecological impacts remain poorly constrained. More importantly, no previous observational study has quantitatively separated the respective contributions of internal-tide-induced vertical advection and turbulent diffusion to nutrient supply in this region. It is still unclear whether internal tides in this region produce a net enrichment of nutrients near the base of the euphotic layer, whether this enrichment is dominated by vertical advection or turbulent diffusion, and how the relative supply of nitrate and silicate may influence phytoplankton community structure. This question is especially relevant because nitrate and silicate do not necessarily have the same vertical distribution or limitation regime, and their relative supply can influence the competitive balance between diatoms and other phytoplankton groups (Brzezinski, 1985; Moore et al., 2013; Ma et al., 2023).

To address this knowledge gap, we combine autonomous glider observations (M'hamdi et al 2025), nutrient fields reconstructed with CANYON-B (ref), and turbulence estimates validated against independent microstructure measurements. This framework enables the first direct comparison between internal-tide-induced vertical advection and turbulent diffusion as nutrient supply mechanisms off the Amazon shelf.

The objectives of this study are therefore threefold. First, we characterize the vertical distribution of nitrate,phosphate and silicate off the Amazon shelf and identify the dominant nutrient limitation regimes within and below the euphotic layer. Second, we isolate and quantify the role of internal-tide-driven vertical advection in modifying nitrate and silicate inventories near the base of the euphotic zone. Third, we estimate the contribution of internal-tide-related turbulent diffusion to nitrate and silicate supply and compare it with the advective pathway. By separating these two mechanisms, this study aims to determine whether internal tides off the Amazon shelf act primarily as a reversible redistribution process or as an irreversible nutrient-supply mechanism.Beyond quantifying nutrient fluxes, we also investigate how internal-tide-induced advection and turbulent diffusion modify the relative supply of nitrate and silicate, providing new insights into their potential influence on nutrient stoichiometry and phytoplankton community structure.

https://doi.org/10.5194/egusphere-2026-4862
Preprint. Discussion started: 19 August 2026


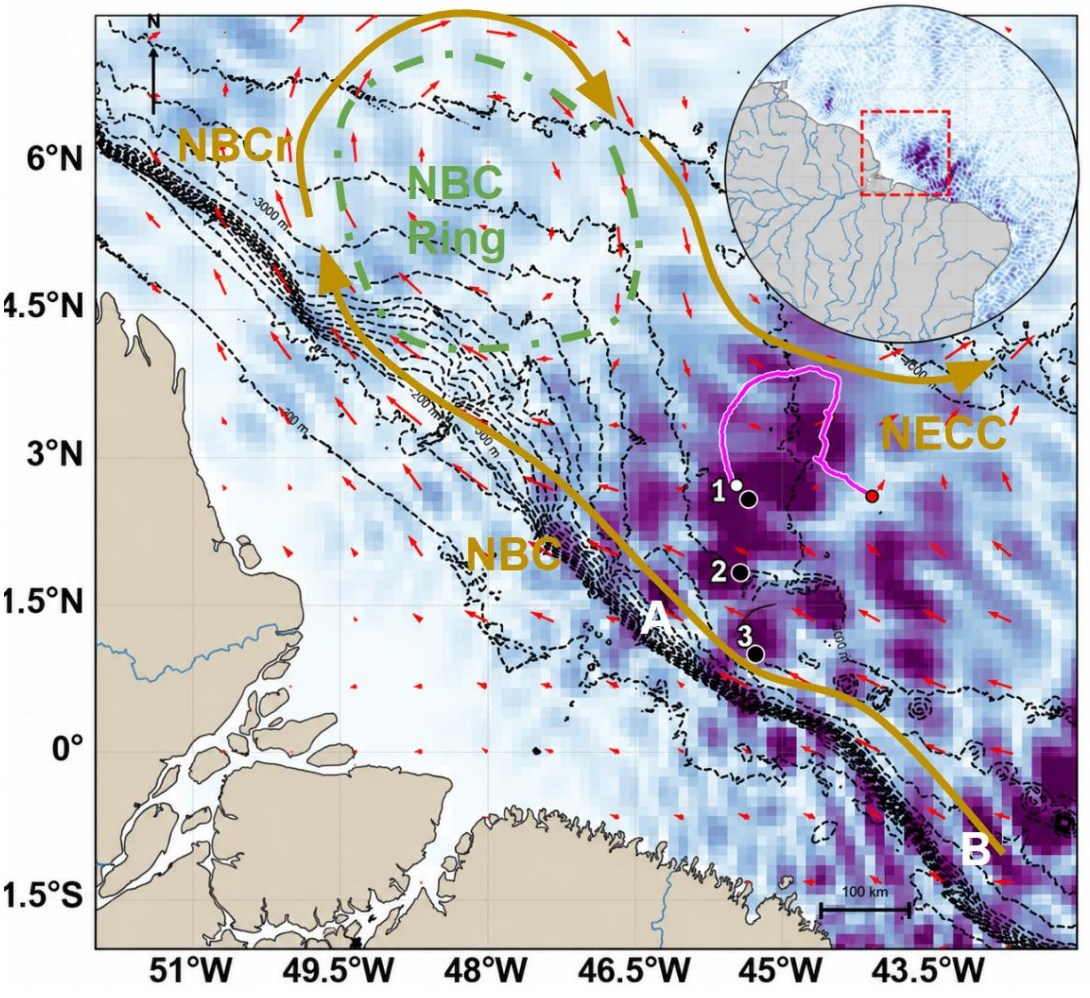


**Figure 1 : Regional map of internal tide anomaly amplitude climatology from MIOST in the AMAZOMIX study area off the Amazon shelf, purple areas mean intense baroclinic signal. Dashed black contours represent bathymetric isobaths. September 2021 surface currents from CMEMS are shown by red arrows, and mean currents are shown in dark yellow (North Brazilian Current, North Brazilian Current retroflexion, North Equatorial Counter Current). The magenta line represents the glider trajectory, with white and red markers indicating the start and end positions, respectively. Black circles labelled 1, 2, and 3 denote the three offshore AMAZOMIX stations. A and B denote Internal Tides generation sites. The NBC ring corresponds to the anticyclonic eddy AE1 identified in M'hamdi et al. (2025).**

## 2 Data and Method

https://doi.org/10.5194/egusphere-2026-4862
Preprint. Discussion started: 19 August 2026


## 2.1 Data

### 2.1.1 AMAZOMIX glider and cruise data

The data used in this study were collected during the AMAZOMIX campaign, a six-week field experiment conducted in three legs aboard the R/V *Antea* from 28 August to 8 October 2021. The campaign was designed to investigate upper-ocean physical–biogeochemical interactions in the western tropical Atlantic. An autonomous underwater glider (Slocum G2) was deployed for 26 days, from 9 September to 5 October 2021, in the oceanic region off northern Brazil, between the North Brazil Current (NBC) and the North Equatorial Countercurrent (NECC) (Figure 1). This region is located along the main internal-tide propagation pathway previously identified by Magalhães et al. (2016), Tchilibou et al. (2022), and Assène et al. (2024).

During the deployment, the glider completed cross-shelf transects, providing quasi-continuous observations of the temporal evolution of the upper water column under varying tidal conditions.The glider collected, high-resolution vertical profiles of hydrographic and biogeochemical properties at a vertical resolution of approximately 1 m, allowing the temporal evolution of the upper water column to be resolved throughout the deployment. The Slocum G2 glider was equipped with a pumped Sea-Bird CTD (temperature, conductivity, and pressure), an Aanderaa optode for dissolved oxygen, and a WetLabs optical puck measuring chlorophyll-*a* fluorescence, colored dissolved organic matter (CDOM), and turbidity. The sensors sampled every 5 s, corresponding to a vertical sampling interval of approximately 1 m. The dataset was processed using the GEOMAR Glider Toolbox (Krahmann, 2023), including thermal-lag correction (Garau et al., 2011), quality control, temporal synchronization, and interpolation onto a regular 1 dbar vertical grid. A complete description of the instrumentation, data processing, and calibration procedures is provided in M'hamdi et al. (2025).

In this study, the glider observations are used primarily to characterize the vertical nutrient structure and its modulation by internal-tide dynamics.. This approach allows both the oscillatory (advective) and irreversible (turbulent diffusive) contributions of internal tides to nutrient supply to be evaluated within a common observational framework. Nitrate, phosphate, and silicate concentrations were reconstructed from the glider hydrographic and oxygen measurements using the CANYON-B neural-network approach of Bittig et al. (2018). The input variables included pressure, temperature, salinity, dissolved oxygen, geographical position, and time of year.

Discrete CTD and nutrient measurements collected at stations A, B, and C during the AMAZOMIX campaign were used to assess the consistency of the CANYON-B-derived nutrient fields, as described in Section 2.1.2. Glider-derived turbulent dissipation rates were also indirectly estimated and evaluated against independent microstructure measurements collected at station A with a VMP-250 Velocity Microstructure Profiler, as described in Section 2.2.3.1. The VMP-250 measured high-frequency temperature and velocity shear microstructure using two FP07 thermistors and two velocity shear probes, providing an independent reference for turbulent kinetic energy dissipation.

Finally, the depth of the euphotic layer (Zeu) , was identified at 125 m, from photosynthetically active radiation (PAR) measurements at station A during AMAZOMIX campaign. Although PAR measurements were available only at this station,

https://doi.org/10.5194/egusphere-2026-4862
Preprint. Discussion started: 19 August 2026


the observed Zeu was considered representative of the study area during the glider deployment and was therefore adopted as a fixed reference depth throughout the analyses.This reference depth was subsequently used to quantify nutrient anomalies and both advective and turbulent nutrient fluxes near the base of the euphotic layer.

### 2.1.1 Nutrient data

Nitrate ($NO_3^-$), phosphate ($PO_4^{3-}$), and silicate ($Si(OH)_4$) concentrations were reconstructed using the CANYON-B method developed by Bittig et al. (2018). CANYON-B, which stands for CArbonate system and Nutrients concentration from temperature salinity and oxygen using a Neural network, is a Bayesian neural-network approach that estimates open-ocean biogeochemical variables from routinely measured hydrographic and oxygen data. In this study, pressure, temperature, salinity, dissolved oxygen, geographical coordinates, and time of year were used as input variables.

The CANYON-B-derived nutrient profiles were compared with in situ nutrient measurements collected at Station 1,2 and 3 during the AMAZOMIX campaign.To quantitatively evaluate the agreement between the observations and the reconstructed nutrient profiles, several statistical metrics were computed, including the mean bias (Bias), root mean square error (RMSE), and Pearson correlation coefficient (r). Overall, the agreement was very good. CANYON-B reproduced the observed nitrate, phosphate, and silicate profiles with very high correlations ($r = 0.992–0.999$), small biases ($-0.04$ to $0.38$ mmol $m^{-3}$), and low RMSE values ($0.05–1.48$ mmol $m^{-3}$). The glider-derived nitrate and phosphate profiles also showed good agreement with bottle measurements, with correlations between 0.91 and 0.97, respectively, low biases ($< 0.06$ mmol $m^{-3}$), and RMSE values below 0.42 mmol $m^{-3}$. These results confirm the overall reliability of both the CANYON-B reconstructions and the glider-derived nutrient profiles for representing the vertical nutrient distributions sampled during the AMAZOMIX campaign.

https://doi.org/10.5194/egusphere-2026-4862
Preprint. Discussion started: 19 August 2026


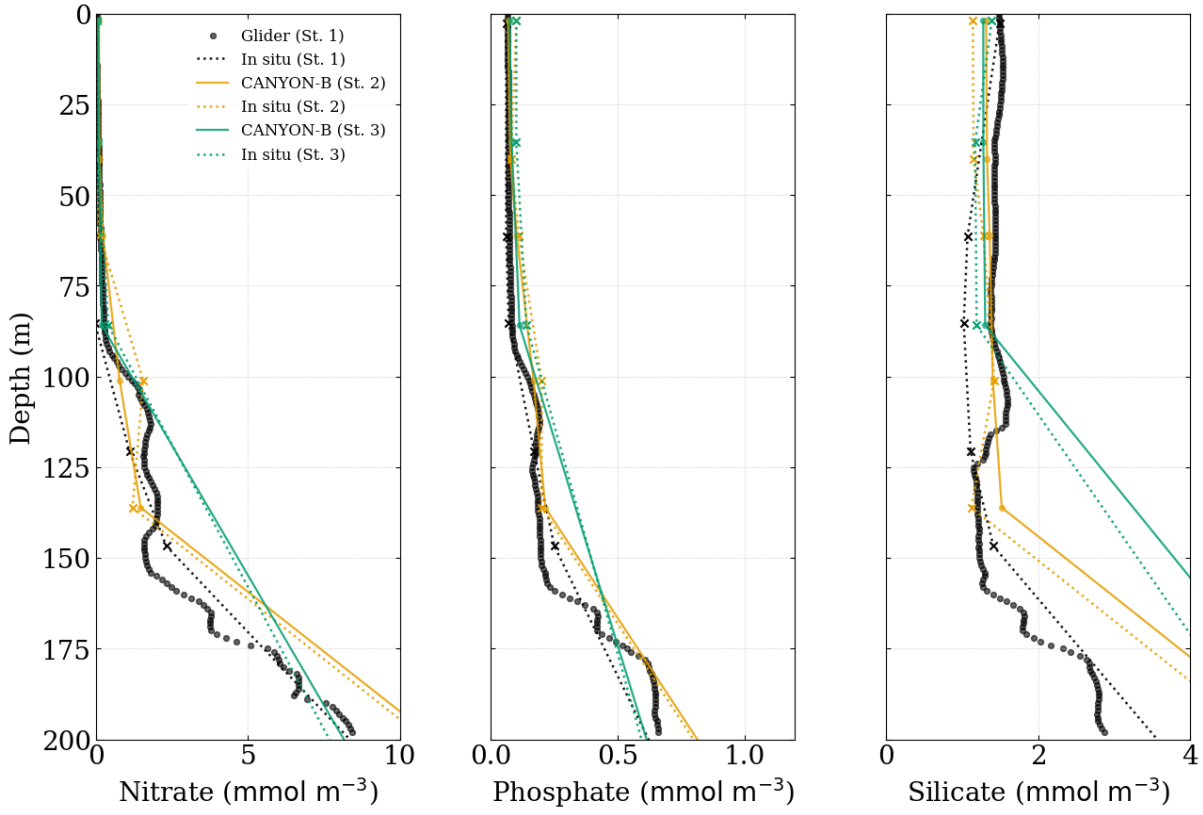


**Figure 2: Comparison of nutrient profiles estimated from Canyon-B with reference profiles (cross) collected during the AMAZOMIX campaign in the glider deployment area. Profiles are shown for nitrate, phosphate, and silicate concentrations. Stations locations are indicated in figure 1**

### 2.1.3 Spring Tides – Neap Tides

Tidal data were extracted from the global FES2014 (Finite Element Solution) model developed by Lyard et al. (2021). The outputs of the sea surface elevation field (eta) were used at the grid point located at 0.75° N, 46° W, corresponding to station A , an internal tide generation site previously identified by Magalhaes et al. (2016) and Tchilibou et al. (2022). The resulting tidal elevation time series was used exclusively to identify spring- and neap-tide periods during the glider deployment (Figure 3). No information derived from the FES2014 model was used in the subsequent nutrient-flux calculations.

https://doi.org/10.5194/egusphere-2026-4862
Preprint. Discussion started: 19 August 2026


## 2.2 Methods

### 2.2.1 Nutrient Availability

To assess the relative availability of nutrients and identify the potentially limiting nutrient throughout the upper water column, nitrate ($NO_3^-$), phosphate ($PO_4^{3-}$), and silicate ($Si(OH)_4$) concentrations were extracted over the 0–200 m depth range. Nutrient concentrations were normalized by reference stoichiometric ratios representative of phytoplankton nutrient demand, with particular emphasis on diatoms. Nitrate and phosphate were evaluated using the classical Redfield ratio of N:P = 16:1. For silicate, we adopted the diatom Si:N uptake ratio of approximately 0.96 or 15/16 reported by Brzezinski et al. (1985). So we used a Si:N:P stoichiometry of 15:16:1.Three relative availability indices for nutrients were then calculated at each measurement point:

$I(NO_3) = [NO_3^-] / 16$,

$I(PO_4) = [PO_4^{3-}] / 1$,

$I(Si) = [Si(OH)_4] / 15$.

At each depth, the nutrient with the lowest index was interpreted as the least available relative to biological demand, and therefore as the potentially limiting nutrient. For graphical comparison, the three indices were subsequently normalized between 0 and 1 by dividing each value by the maximum index among the three nutrients at the same measurement point. A normalized value of 1 therefore indicates the most relatively available nutrient, whereas the lowest normalized value identifies the potentially limiting nutrient while preserving the relative hierarchy among nutrients. The normalized indices were then binned into 5-m depth intervals, and the median value within each bin was computed to reduce the influence of small-scale variability. The resulting vertical profiles were used to visualize depth-dependent shifts in potential nutrient limitation (Figure 9).

### 2.2.2 Nutrient Advection by Internal Tides

The contribution of internal-tide-driven vertical advection to nitrate supply within the euphotic layer was quantified using a simple vertical-advective displacement model (eq.1). Rather than directly estimating vertical velocities, the approach quantifies the vertical displacement of nutrient profiles associated with internal-tide-induced isopycnal oscillations. Internal-tide vertical velocities were inferred from temporal variations in the depth of the $\sigma_0$ = 23.7 kg $m^{-3}$ isopycnal, selected as a conservative and dynamically relevant reference surface because it coincides with the depth of the deep chlorophyll maximum (DCM) during the deployment, allowing the internal-tide-induced isopycnal heaving to be directly related to vertical displacements of the biologically active layer (Figure 4).

For each glider profile, the depth of the $\sigma_0$ = 23.7 kg $m^{-3}$ isopycnal was determined by linear interpolation of potential density as a function of depth. The resulting isopycnal-depth time series was band-pass filtered to isolate the semidiurnal

https://doi.org/10.5194/egusphere-2026-4862
Preprint. Discussion started: 19 August 2026


internal-tide signal before phase identification. Specifically, a fourth-order Butterworth band-pass filter was applied over the 10–18 h period band, encompassing the dominant semidiurnal tidal variability.

The filtered isopycnal-depth time series was then used to identify three characteristic states of the internal-tide cycle: (i) crest, corresponding to the maximum upward displacement of the isopycnal; (ii) trough, corresponding to the maximum downward displacement; and (iii) a neutral state, defined by negligible isopycnal displacement and therefore representative of conditions with little or no internal-tide influence. This classification enabled us to compare the nutrient stock under maximum internal-tide forcing with those observed in the absence of significant internal-tide activity. For each crest–trough sequence, the neutral phase was defined as the profile closest in time to $M_2/4$, equivalent to 3 h 06 min for a semidiurnal tidal period. This phase-based compositing approach isolates the oscillatory signal associated with internal tides while minimizing the influence of lower-frequency variability, including mesoscale circulation and background hydrographic changes. As a result, differences among crest, neutral, and trough profiles can be primarily attributed to internal-tide-induced vertical displacements (Figure 3).

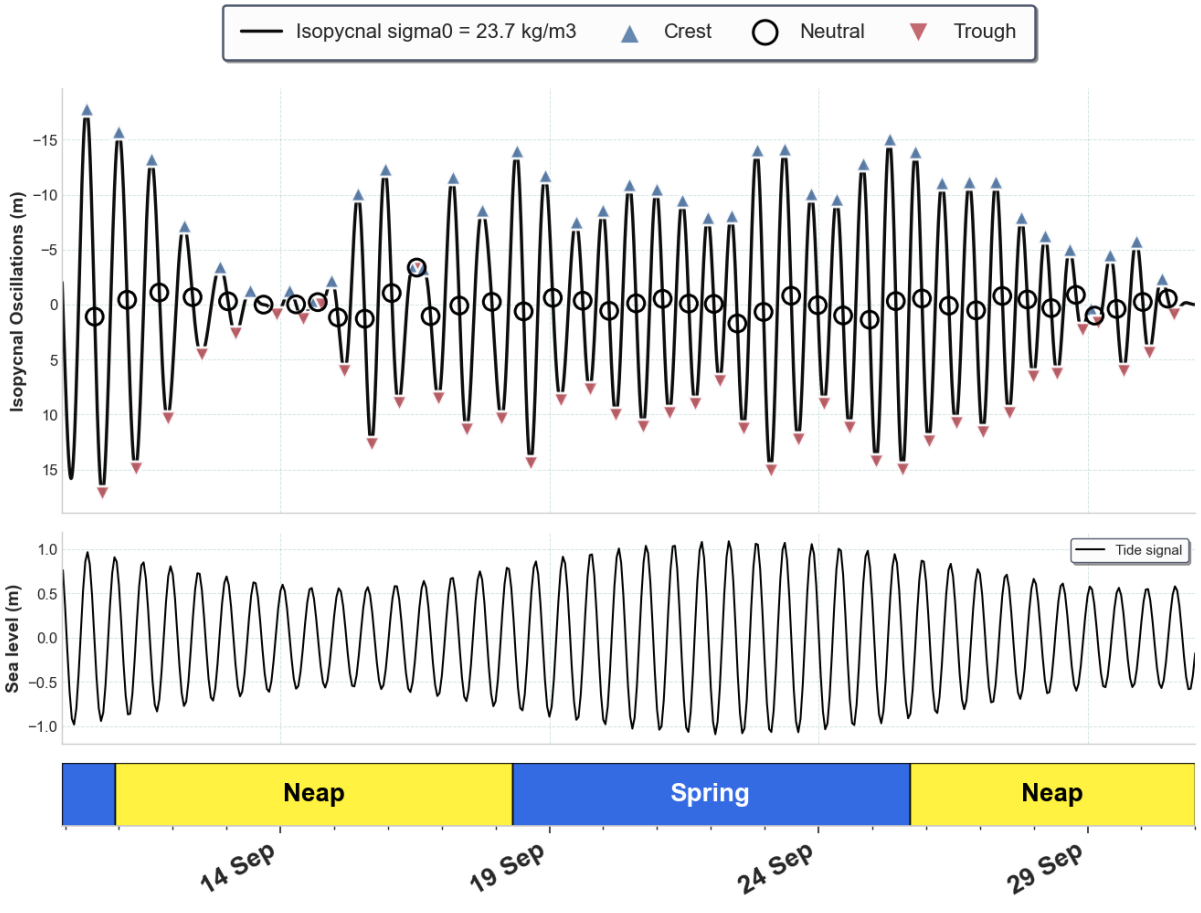

https://doi.org/10.5194/egusphere-2026-4862
Preprint. Discussion started: 19 August 2026


**Figure 3 : Vertical displacement of the 23.7 kg m⁻³ isopycnal along the glider transect, filtered with a 10–18 h Butterworth pass-band filter, and its associated spring–neap tidal modulation using FES2014.**

#### 2.2.2.1 Isolation of nutrient vertical advection driven by internal tides

To isolate the vertical advective component of the nitrate and silicate signals, we compared observed glider profiles with profiles generated using a simple vertical isopycnal advection model. The analysis was restricted to spring tide events, when internal-tide displacements were expected to be strongest. First, the nitracline depth was estimated for each profile as the depth of the maximum vertical nitrate gradient after applying a rolling median filter. Neutral–crest–trough triplets were then identified from the temporal evolution of the nitracline: the crest corresponded to a local minimum in nitracline depth, the trough to the following local maximum, and the neutral profile to the profile closest in time to the midpoint between them. For each triplet, the observed neutral nitrate and silicate profiles were used as reference profiles $P_{Neutral}$ Internal-tide advection was represented as a vertical displacement of these profiles according to:

$$P_{Adv}(z,t) = P_{Neutral}(z + wt) \quad (1)$$

This formulation assumes that nutrient concentrations behave as passive tracers during the short semidiurnal tidal cycle, such that the observed changes in nutrient profiles primarily reflect vertical isopycnal displacements rather than biological uptake, remineralization, or other biogeochemical transformations.

with w, the vertical displacement, positive or negative depending on the direction of the vertical displacement. A negative or positive value of w thus generates either the trough profile, $P_{Trough}$ or crest profile $P_{Crest}$. The displacement was applied over T=3h06 and the prescribed displacement velocity ( ±5 m $h^{-1}$) was derived empirically from the observed migration of the nitracline between successive crest and trough phases during spring tide events. It therefore represents the nutrient effective displacement velocity rather than an measured vertical velocity. Mean profiles and interquartile ranges were then calculated separately for the modeled and observed crest, neutral, and trough profiles for both nitrate and silicate, allowing the advective response predicted by the model to be directly compared with the nutrient variability measured by the glider (Figure 5).

https://doi.org/10.5194/egusphere-2026-4862
Preprint. Discussion started: 19 August 2026


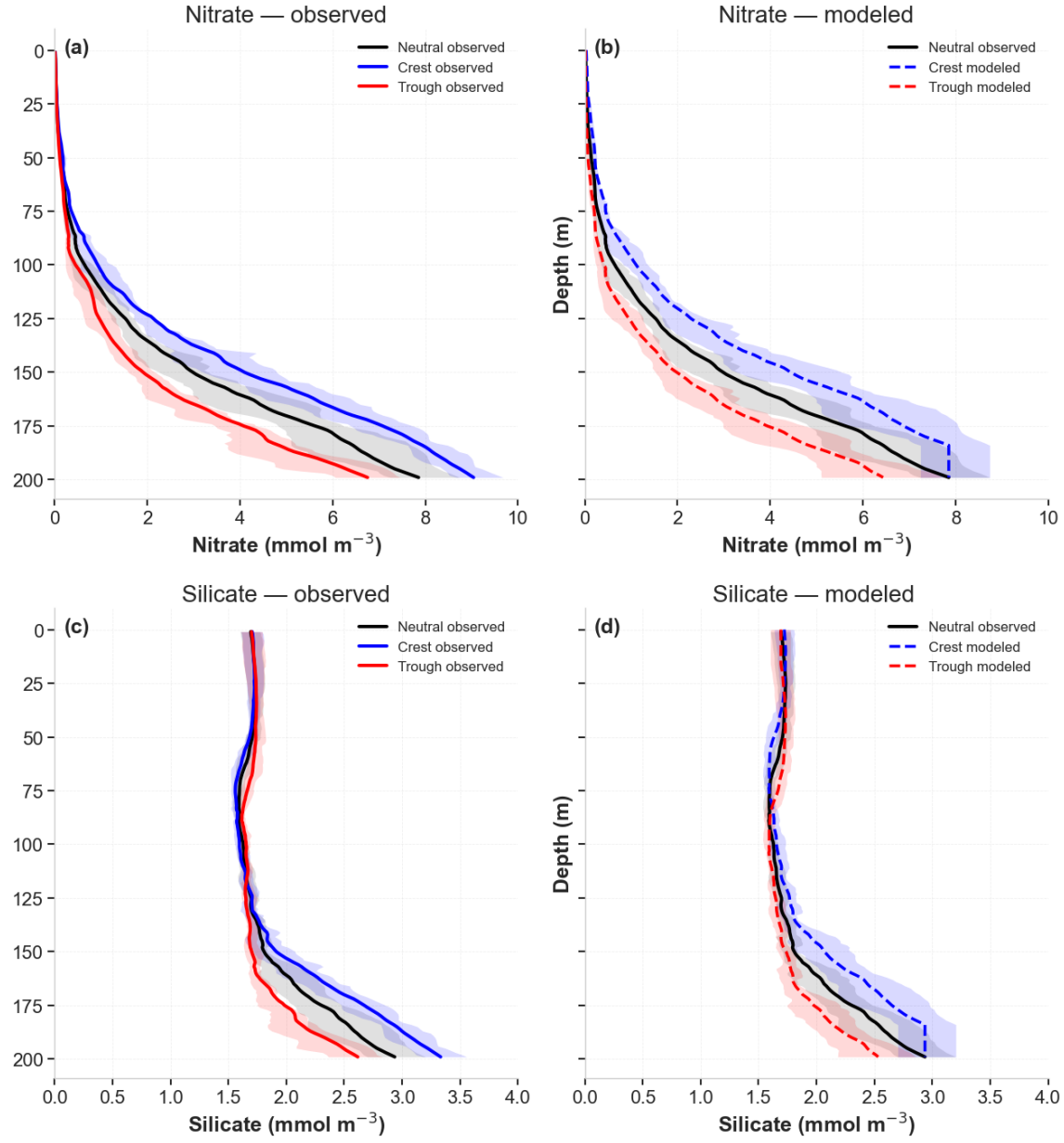


**Figure 4 : Mean spring-tide impact of internal-tide-induced vertical advection on nitrate and silicate profiles. (a) and (b) show nitrate profiles and (c) and (d) show silicate profiles. Left panels show the observed response for neutral, crest, and trough tidal phases, while right panels show the corresponding mean modeled profiles for the same phases.**

https://doi.org/10.5194/egusphere-2026-4862
Preprint. Discussion started: 19 August 2026


#### 2.2.2.2 Isolation of nutrient vertical advection driven by internal tides

For a vertically structured nutrient profile, symmetric upward and downward displacements do not necessarily produce symmetric changes in the nutrient inventory sampled within a fixed layer around Zeu due to the non linear nutrient profile with depth. When the profile is convex, the increase in nutrient concentration caused by the upward displacement of deeper, nutrient-rich waters is larger than the decrease caused by the downward displacement. As a result, the average of the crest and trough configurations exceed the neutral configuration, even if the vertical displacements are symmetric as illustrated in Figure 5 in consistent with Jensen's inequality (Jensen et al 1906).

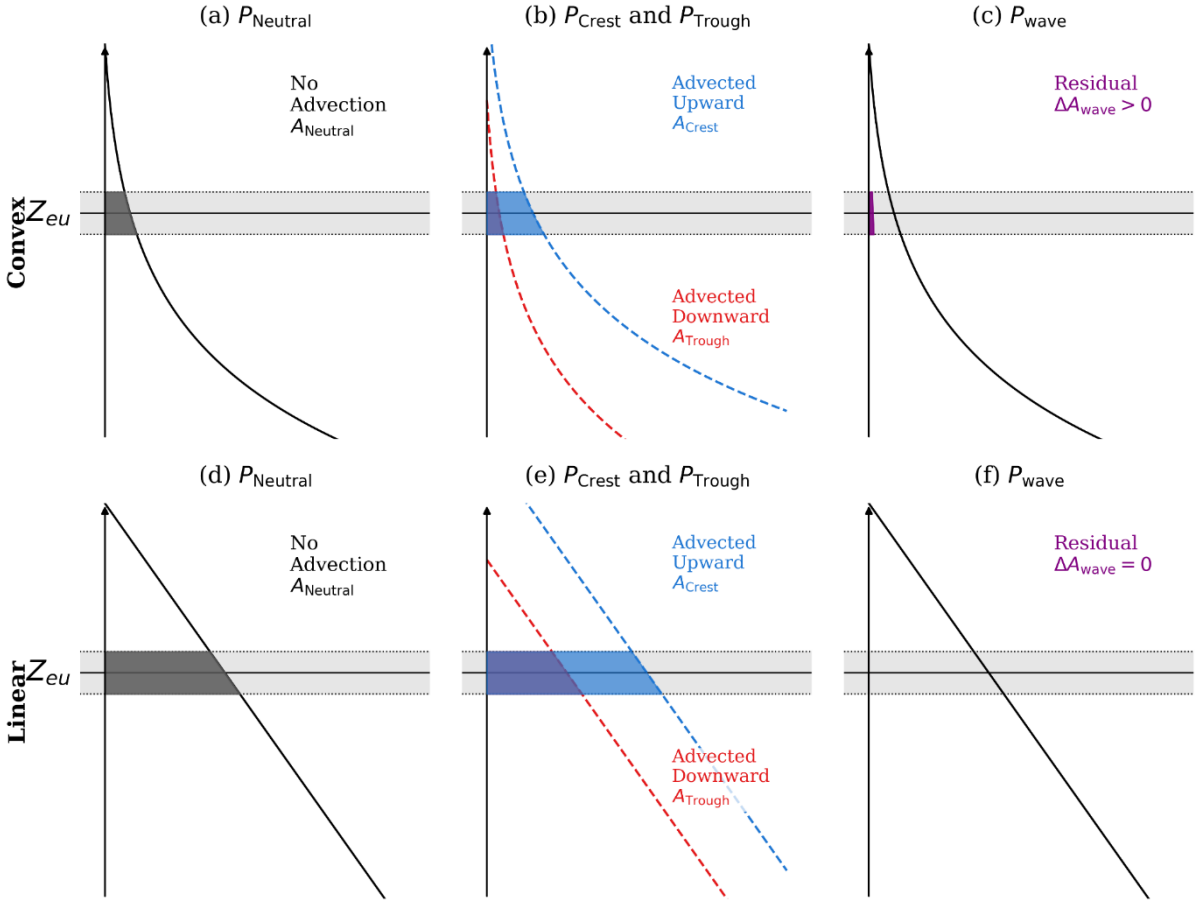


**Figure 5 : Impact of internal tide advection on a typical nutrient profile. Ai (i = neutral, crest or trough) corresponds to the integrated area within the Zeu + 5 m and Zeu − 5 m zone.**

The mean area sampled over one internal-wave tidal cycle was estimated as the average between the crest and trough configurations:

https://doi.org/10.5194/egusphere-2026-4862
Preprint. Discussion started: 19 August 2026


$$P_{wave} = (P_{crest} + P_{trough}) / 2 \quad (2)$$

The net wave-induced excess relative to the neutral in Zeu was then computed as

$$\Delta A_{wave} = \int_{Z_{eu}-10}^{Z_{eu}+10} \left(P_{(wave)(z)} - P_{(neutral)(z)}\right) dz \quad (3)$$

This quantity represents the mean contribution of vertical advection by internal tides within the $Z_{eu}$ layer over one tidal cycle. To express this contribution as a daily advective flux, $\Delta A_{wave}$ was multiplied by the number of tidal cycles per day:

$$F_{ADV} = \Delta A_{wave} \times (24 / T_{tides}) \quad (4)$$

where $T_{tides}$ is the tidal period in hours.

In this study, this method was applied to the mean spring-tide profiles in order to estimate the average advective flux associated with internal tides.

### 2.2.3 Nutrient Diffusion by Internal Tides

#### 2.2.3.1 Estimation of Turbulent Kinetic Dissipation

Turbulent kinetic energy dissipation rate, ε, was estimated from the glider observations using the Large Eddy Method (LEM; Beaird et al., 2012), following the adaptation proposed by Evans et al. (2018). This approach provides an indirect estimate of turbulent dissipation from glider-derived observations, enabling turbulence to be evaluated continuously along the entire glider transect where direct microstructure measurements are unavailable. The LEM assumes a steady turbulent energy cascade, in which the dissipation rate scales with a turbulent velocity scale, q′, and a turbulent length scale, l, such that $\varepsilon \sim (q')^3/l$. Using the Ozmidov length scale as the relevant turbulent length scale yields $\varepsilon = C\varepsilon\, N(q')^2$, where N is the buoyancy frequency and Cε is a proportionality constant calibrated against in situ microstructure measurements, here obtained with the VMP.

In LEM, the turbulent velocity scale q′ is computed from the filtered vertical velocity. Water vertical velocities were retrieved using the open-source *GliderFlight* package (Merkelbach, 2019), which implements the dynamic flight model following the methodology described by Merkelbach et al. (2018).Unlike the original implementation of Beaird et al. (2012), which used a fixed 30-m cutoff wavelength to filter vertical velocities, we followed Evans et al. (2018) and applied an adaptive cutoff based on the local buoyancy frequency, N. This approach improves the separation of turbulent motions from low-frequency internal-wave variability under variable stratification. The turbulent velocity scale q′ was then computed as the root-mean-square of the filtered vertical velocity, and ε was estimated in 20-m vertical bins.

Glider-derived dissipation estimates were evaluated against concurrent microstructure measurements collected with a VMP at the glider deployment site during the AMAZOMIX campaign. Figure 6 demonstrates that the LEM reproduces both the vertical structure and the order of magnitude of ε.

Because the LEM is not valid to describe unstratified mixed-layer turbulence, it shows poor agreement with observations in the upper approximately 70 m (Evans et al., 2018), this depth range was excluded from subsequent analyses. This depth layer being away from the nutriclines, it does not impact our analysis. Between 70 and 200 m, comparison with VMP

https://doi.org/10.5194/egusphere-2026-4862
Preprint. Discussion started: 19 August 2026


observations yields a small mean bias (−0.094 in log10 space, corresponding to a mean underestimation of approximately 19%). In addition, 70% of the glider-derived ε estimates fall within the variability envelope defined by the VMP observations, indicating that most of the glider profile remains consistent with the observed turbulence variability. The LEM also reproduces the vertical structure reasonably well (Spearman's $\rho = 0.56$, $p < 0.001$), supporting its application to the complete glider dataset.

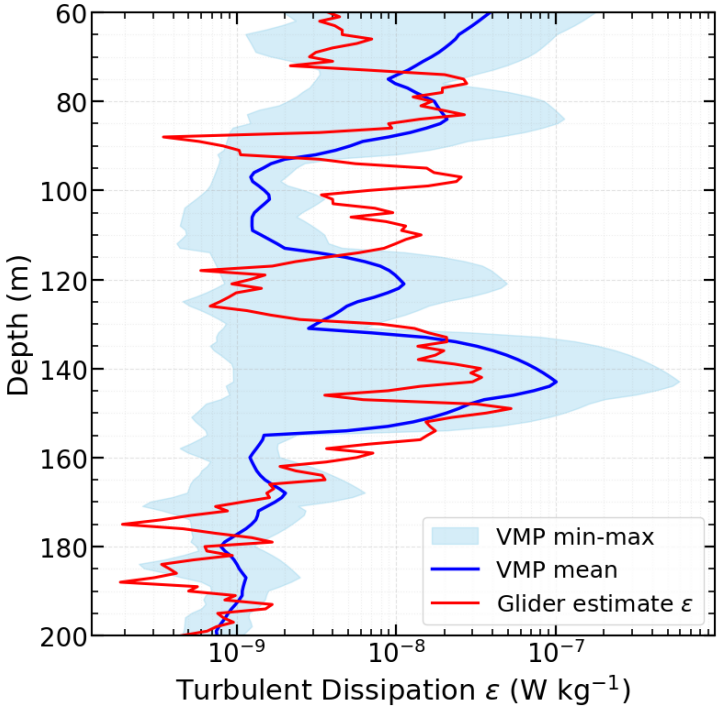


**Figure 6 : Turbulent kinetic energy dissipation rate, ε, measured during the AMAZOMIX campaign and estimated from glider observations using the large-eddy method of Evans et al. (2018).**

#### 2.2.3.2 Turbulent Nutrient Fluxes

Vertical turbulent nutrient fluxes were estimated using a Fickian diffusion framework. The diapycnal diffusivity Kz was first derived from dissipation rate estimates using the Osborn (1980) relation:

$$Kz = \Gamma \varepsilon / N^2 \quad (5)$$

where $\Gamma = 0.2$ is the mixing efficiency, ε is the turbulent kinetic energy dissipation rate, and $N^2$ is the squared buoyancy frequency computed from the smoothed density profile. The local turbulent nutrient flux was then estimated as:

$$F(z) = -Kz(z)\, \partial C(z)/\partial z \quad (6)$$

where C represents either nitrate or silicate concentration, Kz(z) is the vertical turbulent diffusivity, and $\partial C(z)/\partial z$ is the local vertical nutrient gradient. The gradient was computed by finite differencing adjacent depth levels within each glider profile. Nutrient gradients were calculated separately for nitrate and silicate. In this formulation, z is defined as positive upward.

https://doi.org/10.5194/egusphere-2026-4862
Preprint. Discussion started: 19 August 2026


Therefore, positive flux values correspond to a nutrient increase due to vertical turbulent diffusion, from deeper waters enriched in nutrients toward the euphotic layer. The resulting F(z) represents the local turbulent diffusive flux at each depth level. It was then converted to a daily flux by multiplying by the number of seconds per day:

$$F_{day}(z) = F(z) \times 86400 \quad (7)$$

with $F_{day}$ expressed in mmol $m^{-2}$ $d^{-1}$. To obtain a single diffusive flux value comparable with the internal-tide-driven advective contribution, the daily flux was averaged over the depth interval corresponding to the base of the euphotic zone:

$$F_{Diff} = \frac{1}{20}\int_{Zeu-10}^{Zeu+10} F_{(day)(z)dz} \quad (8)$$

Thus, $F_{DIFF}$ represents the mean daily turbulent diffusive nutrient flux across the Zeu layer and was calculated separately for nitrate and silicate.

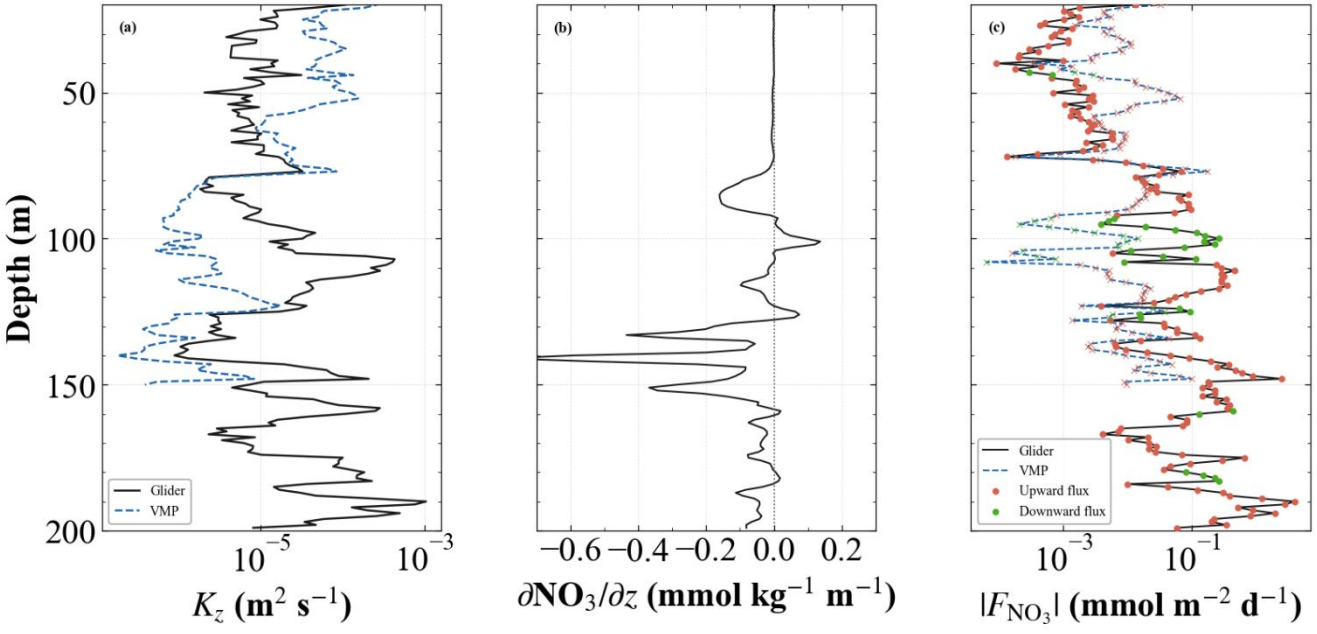


**Figure 7: Glider-derived estimates of vertical diffusivity, of the vertical nitrate gradient, and turbulent nitrate flux for a representative profile collected on 9 September 2021, compared with VMP-derived Kz and the associated turbulent nitrate flux.**

Overall, by expressing both the advective flux, $F_{ADV}$, and the turbulent diffusive flux, $F_{DIFF}$, in mmol $m^{-2}$ $d^{-1}$ at the base of the euphotic layer, this methodology allows the relative contributions of internal-tide-driven vertical advection and turbulent diffusion to nitrate and silicate supply to be directly compared.

The turbulent nutrient fluxes estimated here represent the total turbulent transport. In the Discussion, only the fraction attributed to internal tides is considered when comparing turbulent diffusion with internal-tide-induced advection. Following Kouogang et al. (2025), who estimated that internal tides account for approximately 50% of the observed turbulent

https://doi.org/10.5194/egusphere-2026-4862
Preprint. Discussion started: 19 August 2026


dissipation at Station 1,2 and 3, this fraction is used as a first-order approximation of the internal-tide-related turbulent nutrient flux

## 3 Results

### 3.1 Nutrients Vertical Distribution

The vertical nutrient profiles reveal a marked structuring of nutrient availability between the surface and 200 m (Figure 8). Nitrate and phosphate show similar vertical patterns, with low surface concentrations of approximately 0.2 mmol $NO_3$ $m^{-3}$ and 0.2 mmol $PO_4$ $m^{-3}$, consistent with nutrient depletion within the euphotic layer. Both nutrients then increase progressively with depth, reaching approximately 3 mmol $NO_3$ $m^{-3}$ and 0.45 mmol $PO_4$ $m^{-3}$ at 125 m, near the base of the euphotic zone.

In contrast, silicate exhibits a more heterogeneous vertical distribution, with relatively high surface concentrations ranging from 1 to 2 mmol Si $m^{-3}$. Concentrations decrease to a minimum of approximately 0.6 mmol Si $m^{-3}$ at around 75 m before increasing again at greater depths. The mean profiles shown in Figure 8 further emphasize these contrasting patterns. Nitrate is nearly depleted at the surface and increases steadily downward, whereas silicate shows two distinct decreases, first between 50 and 75 m and then between 125 and 150 m. These differences indicate that nitrate and silicate do not follow the same vertical dynamics, despite both contributing to the relative nutrient availability structure described below. The normalized relative availability indices confirm this vertical differentiation (Figure 9).

In the upper layer, down to approximately 80–90 m, nitrate exhibits the lowest normalized values, indicating that it is the least available nutrient relative to phytoplankton biological requirements. Below this depth, the dominant nutrient limitation shifts from nitrate to silicate.This decrease becomes particularly pronounced below 120 m, where the normalized silicate index reaches the lowest values of the profile, while nitrate becomes relatively more available.

Phosphate remains close to 1 throughout the water column, suggesting that it is not the least available nutrient in this region. Overall, the water column is characterized by a vertical transition from relative nitrate limitation in the upper layer to relative silicate limitation in the deeper part of the euphotic zone and below. This pattern may reflect silicate uptake by silicifying organisms, particularly diatoms, near the base of the euphotic layer. The nutricline depths are broadly consistent among nutrients, with minor variations around 140 m. However, the silicate nutricline is located deeper, around 185 m, indicating a partial decoupling between deep silicate enrichment and nitrate–phosphate enrichment. These observations indicate different vertical distributions of nitrate and silicate within the water column.

Nitrate and phosphate appear to be uplifted higher in the water column than silicate, consistent with the deeper depth of the silicate nutricline. This vertical organization occurs within a hydrodynamic context characterized by strong internal-tide activity. Vertical oscillations of iso-nutrient surfaces, particularly around the nutriclines, suggest that internal tides may periodically promote nutrient injection toward the euphotic zone. The amplitude of these oscillations differs between spring- and neap-tide periods, potentially creating repeated windows of enhanced nutrient supply to the illuminated layer.

https://doi.org/10.5194/egusphere-2026-4862
Preprint. Discussion started: 19 August 2026


370 The following analysis therefore aims to quantify the respective contributions of vertical advection and turbulent diffusion associated with internal tides to nitrate and silicate supply toward the euphotic zone.

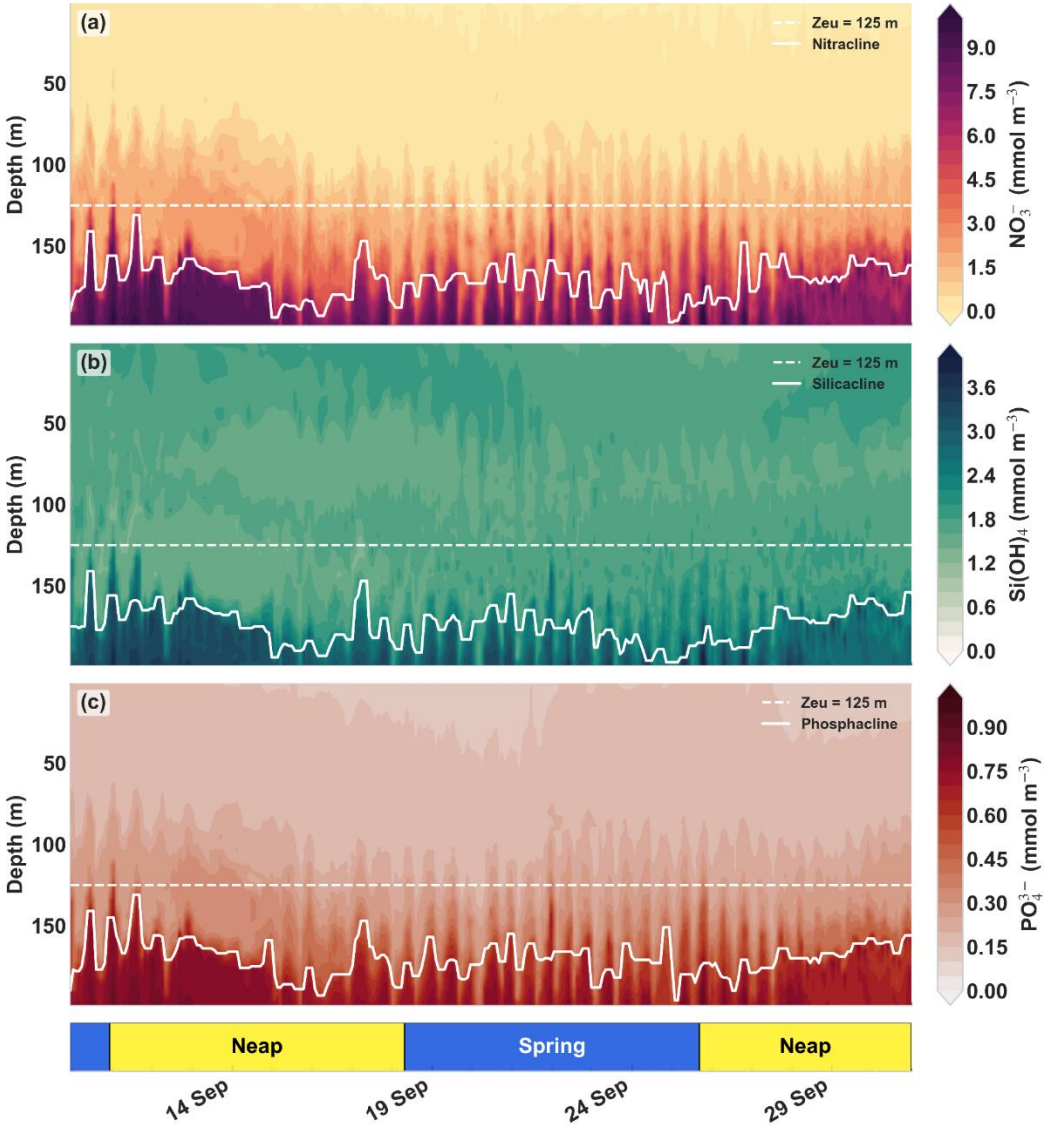


**Figure 8 : Time–depth distributions of nitrate, silicate, and phosphate estimated from Canyon-B glider observations during the** 375 **AMAZOMIX campaign. The white solid lines indicate the depth of the maximum vertical gradient for each nutrient, corresponding to the nitracline, silicacline, and phosphacline, respectively. The white dashed line marks the fixed euphotic depth. Concentrations are expressed in mmol m $^{-3}$**

380

https://doi.org/10.5194/egusphere-2026-4862
Preprint. Discussion started: 19 August 2026


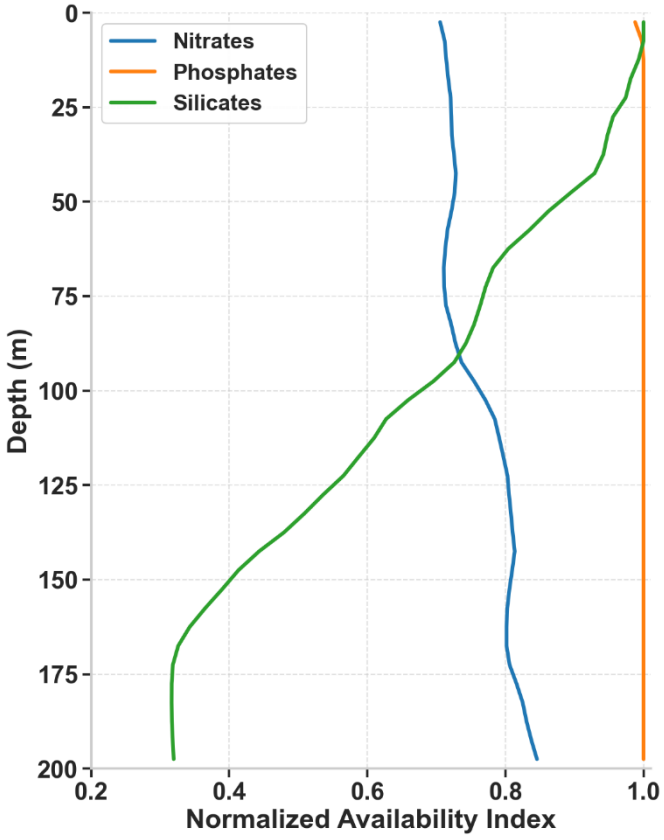


**Figure 9 : Vertical profiles of normalized indices of relative nitrate, phosphate, and silicate availability between 0 and 200 m. The indices were calculated from the reference stoichiometric ratios $NO_3$ = 16:1:16, then normalized at each point by the maximum value among the three nutrients. The curves represent medians computed over 5 m depth bins. Lower values indicate the relatively least available nutrient and therefore the potentially limiting nutrient.**

### 3.2 Nutrient Vertical advection by internal tides

To isolate the vertical advection of internal tides, nutrient anomalies were analysed relative to the neutral tidal phase as described in Section 2.2.2. The vertical distribution of these anomalies are shown in Figures 10a and 10b and closely reflects the background nutricline structure. Above the euphotic depth (Zeu), which corresponds approximately to the onset of the nutricline inflection, anomalies remain relatively weak. In contrast, they become much more pronounced below Zeu, where vertical nutrient gradients are steeper. Over the full 0–200 m depth range, anomaly amplitudes generally remain below 1 mmol $NO_3$ $m^{-3}$ for nitrate and below 0.3 mmol Si $m^{-3}$ for silicate, indicating that the nutrient response is constrained by both the amplitude of vertical displacement and the local background nutrient gradient. A spring–neap modulation is also observed. Positive nutrient anomalies occur with higher intensities during spring-tide periods, coincident with periods

https://doi.org/10.5194/egusphere-2026-4862
Preprint. Discussion started: 19 August 2026


of enhanced internal-tide activity promoting the upward displacement of nutrient-rich waters toward the base of the euphotic layer. Above Zeu, spring-tide conditions are associated with positive anomalies reaching approximately 0.5 mmol $NO_3$ $m^{-3}$ and 0.04 mmol Si $m^{-3}$, whereas neap-tide anomalies are typically about two times weaker. Negative anomalies of comparable magnitude are also observed, consistent with alternating upward and downward phases of the internal tide. The integrated time series of advective nutrient anomalies at the base of the euphotic zone, computed over the 115–135 m depth interval, is shown in Figure 10c. Nitrate anomalies are shown in red and silicate anomalies in green. Both tracers exhibit marked short-term variability, with rapid alternations between enrichment and depletion events relative to the neutral profile. Integrated nitrate anomalies vary approximately between −10 and +8 mmol $NO_3$ $m^{-2}$, whereas silicate anomalies range from about −2.5 to +2 mmol Si $m^{-2}$, excluding the very large initial positive event. During spring tides, positive nitrate and silicate anomalies occur more regularly, although their amplitudes remain variable. Nitrate enrichment commonly reaches a few mmol $NO_3$ $m^{-2}$, with peaks of approximately 5–8 mmol $NO_3$ $m^{-2}$, while silicate anomalies are generally smaller but frequently positive. In contrast, during neap tides, anomalies are more often close to zero or negative, particularly during the first neap period, when nitrate anomalies decrease to around −6 mmol $NO_3$ $m^{-2}$ and silicate anomalies also indicate depletion.

These observations were subsequently quantified by averaging the integrated anomalies over the spring- and neap-tide periods, allowing the net advective contribution associated with internal-tide activity to be estimated.

https://doi.org/10.5194/egusphere-2026-4862
Preprint. Discussion started: 19 August 2026


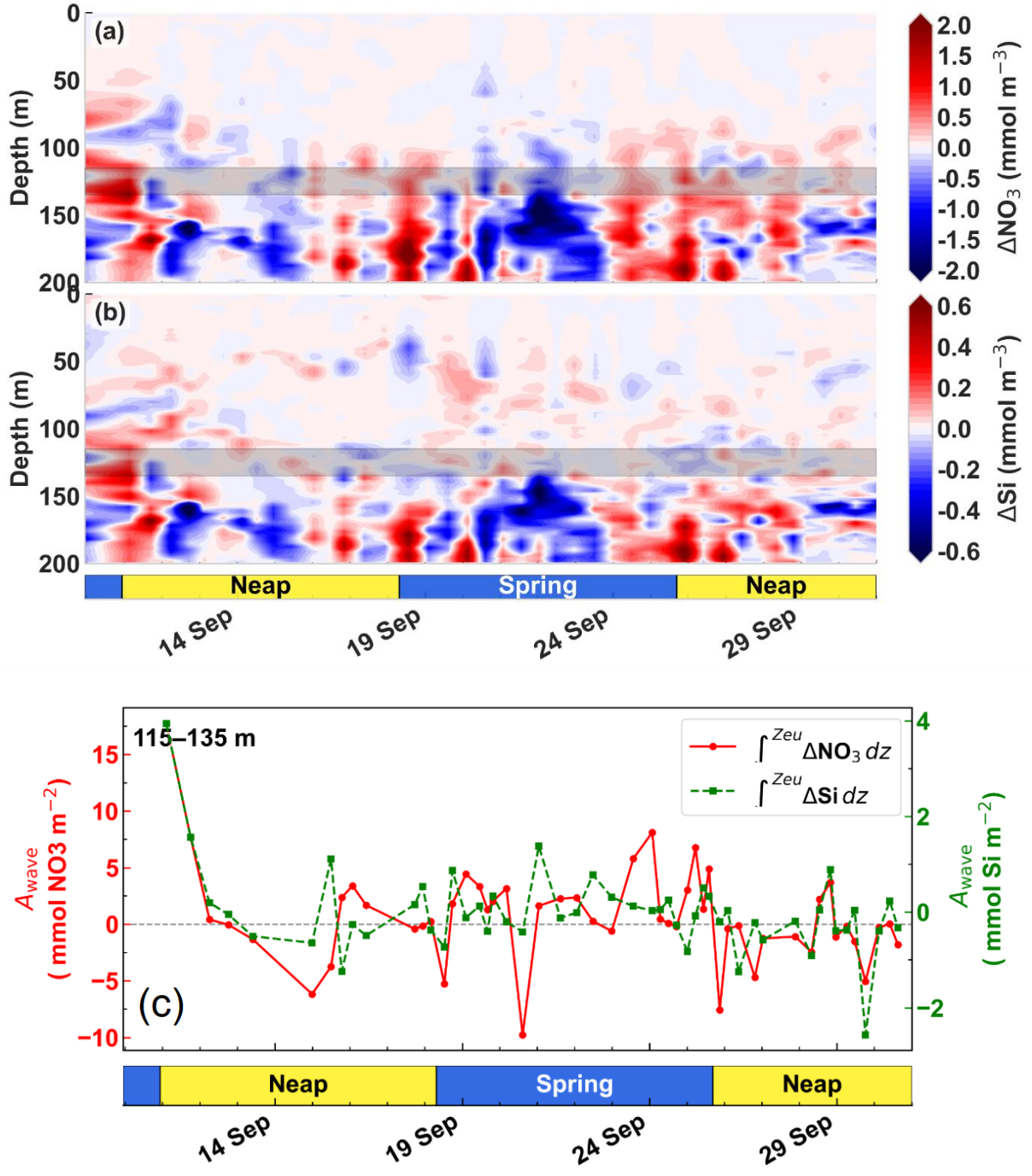


**Figure 10 : (a, b) Hovmöller diagrams of observed nutrient anomalies associated with internal tide displacements between the surface and 200 m depth. Anomalies were computed for each detected crest–neutral–trough triplet as the difference between the mean crest–trough profile and the neutral profile, i.e., $\Delta = [(P_{Crest} + P_{Trough})/2] - P_{Neutral}$. Panels show anomalies in (a) nitrate and (b) silicate concentrations. Positive values indicate enrichment relative to the neutral profile, while negative values indicate depletion. The grey shaded band highlights Zeu. (c) Time series of integrated nitrate and silicate anomalies between 115 - 135 m layer. The red curve represents $\Delta NO_3$, plotted on the left y-axis, while the green curve represents ΔSi**

https://doi.org/10.5194/egusphere-2026-4862
Preprint. Discussion started: 19 August 2026


When the anomalies are averaged by tidal period, a positive anomaly emerges at the base of the euphotic layer during spring tides, whereas the neap-tide signal remains weak and negative (Figure 11). This result supports the theoretical framework presented in Section 2.2.2.2, which predicts that internal-tide oscillations can generate a net nutrient anomaly near the lower boundary of Zeu, with a magnitude strongly controlled by spring–neap modulation of internal-tide activity. The vertically integrated anomaly is hereafter denoted $\Delta A_{wave}$. During spring tides, $\Delta A_{wave}$ reaches 1.19 mmol $NO_3$ $m^{-2}$ for nitrate and 0.19 mmol Si $m^{-2}$ for silicate. When converted to a daily timescale using the tidal period, these values correspond to an advective nutrient supply of 2.3 mmol $NO_3$ $m^{-2}$ $d^{-1}$ and 0.4 mmol Si $m^{-2}$ $d^{-1}$. the spring-tide nutrient supply is approximately 4.6 times higher for nitrate ( 0.5 mmol $NO_3$ $m^{-2}$ $d^{-1}$) and 4 times higher for silicate (0.1 mmol Si $m^{-2}$ $d^{-1}$). The weaker neap-tide signal is used here to define an uncertainty range around the spring-tide estimate, yielding $F_{ADV}$ = 2.3 ± 0.5 mmol $NO_3$ $m^{-2}$ $d^{-1}$ and $F_{ADV}$ = 0.4 ± 0.1 mmol Si $m^{-2}$ $d^{-1}$. These estimates indicate that internal-tide-driven vertical advection can provide an intermittent nutrient input at the base of the euphotic layer, with effective enrichment occurring primarily during spring tides.

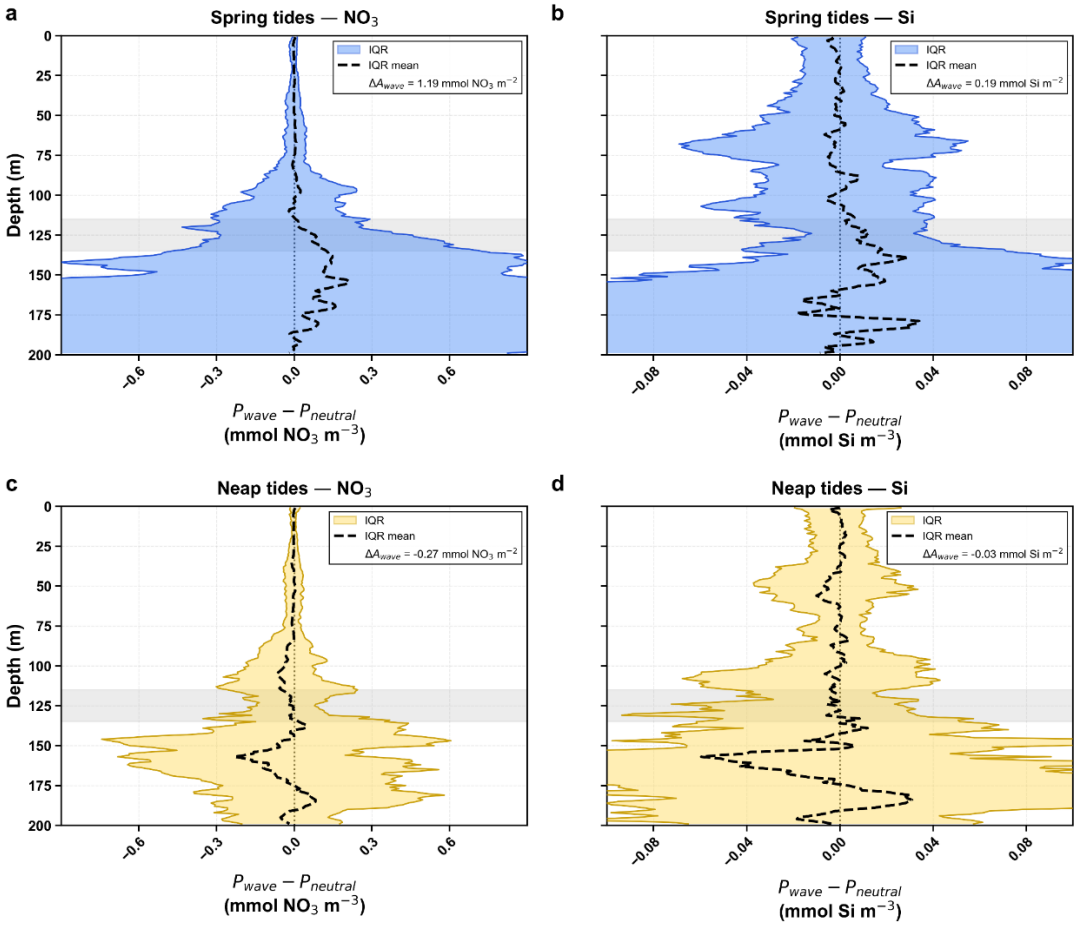


**Figure 11 : Vertical profiles of nutrient anomalies associated with internal tide displacements during spring and neap tidal periods. Panels show nitrate and silicate anomalies for spring tides and neap tides between 0 and 200 m depth. The purple**

https://doi.org/10.5194/egusphere-2026-4862
Preprint. Discussion started: 19 August 2026


**envelope represents the interquartile range (Q1–Q3) of the anomalies across all triplets, The grey shaded band marks Zeu band layer used to compute the integrated $\Delta A_{wave}$.**

### 3.3 Nutrient Vertical diffusion by internal tides

The turbulent dissipation rate estimated from the LEM is shown in Figure 12. Values mainly range between $10^{-9}$ and $10^{-7}$ W kg$^{-1}$, with a marked vertical structure within the 100–200 m layer, corresponding to the thermocline. In our results, spring-tide periods exhibit a relatively homogeneous vertical distribution of dissipation, with mixing hotspots extending over thicknesses of approximately 40–120 m and dissipation rates ranging from $10^{-8}$ to $10^{-7}$ W kg$^{-1}$. In contrast, neap-tide periods show more localized dissipation signatures, although they can occasionally reach higher intensities, particularly around days 14 and 29. During these neap-tide events, the vertical extent of the dissipation hotspots remains limited and generally does not exceed 40 m. These turbulent dissipation rates were subsequently used to estimate vertical turbulent nutrient fluxes F(z) (equation 6 in Section 2.2.3.2). The resulting fluxes are shown in Figure 12.

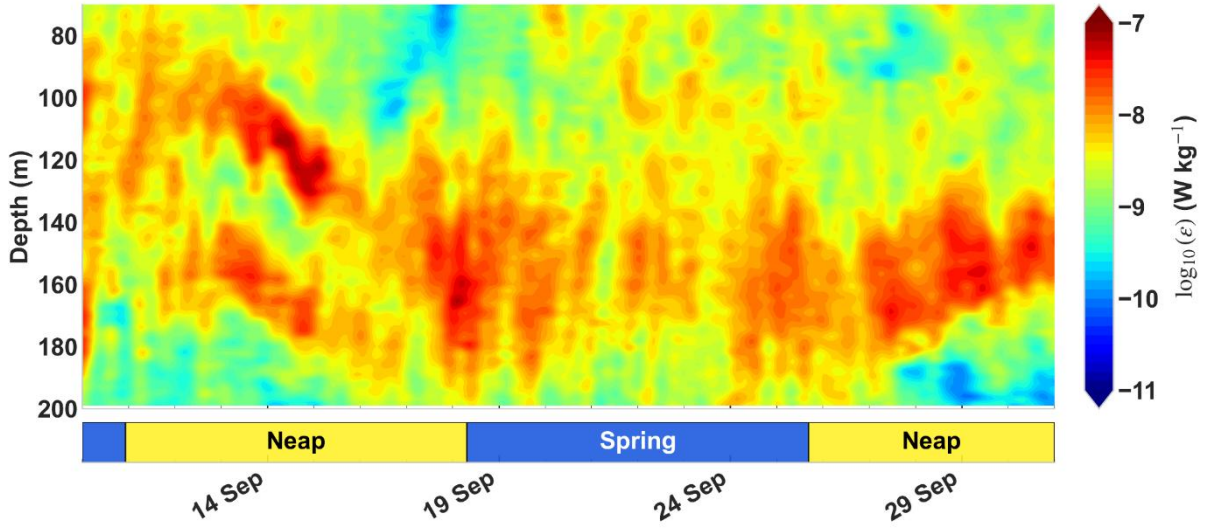


**Figure 12 : Temporal evolution of turbulent kinetic energy dissipation during glider transect between 70 and 200 m depth.**

The turbulent nitrate and silicate fluxes are presented in the upper panels of Figure 13. Similar to the advective anomalies shown in Figure 10, turbulent fluxes are strongest below the euphotic zone and decrease markedly above it, with an approximately threefold reduction near the base of the euphotic layer. This decrease is likely related to weaker nutrient gradients in the upper part of the water column. Nitrate fluxes are shown in Figure 13a and silicate fluxes in Figure 13b. Both nutrients exhibit similar vertical and temporal structures, with the strongest turbulent fluxes located below the euphotic zone, close to the nutricline depth, between approximately 150 and 190 m.

https://doi.org/10.5194/egusphere-2026-4862
Preprint. Discussion started: 19 August 2026


Above the base of the euphotic zone, highlighted by the grey band around 125 m, fluxes are generally weaker. For nitrate, turbulent fluxes typically reach values on the order of 1 mmol $NO_3$ $m^{-2}$ $d^{-1}$, with local maxima of about 1.5 mmol $NO_3$ $m^{-2}$ $d^{-1}$. Silicate fluxes are smaller, generally around 0.2 mmol Si $m^{-2}$ $d^{-1}$, with local maxima reaching approximately 0.4 mmol Si $m^{-2}$ $d^{-1}$. For both nutrients, fluxes are predominantly positive, indicating a net upward turbulent supply from nutrient-rich subsurface waters toward the euphotic layer. The vertical distribution of these fluxes is consistent with the dissipation patterns described above, as the largest turbulent nutrient fluxes occur near the nutriclines and within the thermocline. These information are summarized in table 1.

During spring tides, fluxes show a greater vertical extent and more frequent positive patches, particularly between about 19 and 25 September. During this period, positive turbulent fluxes extend upward from the nutricline toward the base of the euphotic zone, suggesting enhanced vertical connectivity between the nutrient-rich subsurface layer and the lower euphotic layer. In contrast, during neap tides, fluxes are more localized and intermittent, with positive patches mostly confined below the euphotic zone and occasional negative events. These results suggest that spring-tide internal mixing enhances the upward turbulent transport of nitrate and silicate, acting as a nutrient pump that episodically supplies nutrients to the base of the euphotic zone.

| Metric | Nitrate | Silicate |
|---|---|---|
| Mean Turbulent Flux above Zeu | 1 mmol $NO_3$ $m^{-2}$ $d^{-1}$ | 0.2 mmol Si $m^{-2}$ $d^{-1}$ |
| Maximum turbulent flux above Zeu | 1.5 mmol $NO_3$ $m^{-2}$ $d^{-1}$ | 0.4 mmol Si $m^{-2}$ $d^{-1}$ |
| Integrated flux range (115-130 m) | −10 to +13 mmol $NO_3$ $m^{-2}$ $d^{-1}$ | −5 to +5 mmol Si $m^{-2}$ $d^{-1}$ |
| Mean Flux on Spring Tides events | 5–10 mmol $NO_3$ $m^{-2}$ $d^{-1}$ | 2–4 mmol Si $m^{-2}$ $d^{-1}$ |

**Table 1: Summary of the main characteristics of turbulent nutrient fluxes.**

The integrated time series of turbulent nutrient fluxes at the base of the euphotic zone, computed over the 115–135 m depth interval, is shown in Figure 13c, while the main quantitative characteristics are summarized in Table 1. Both nitrate and silicate fluxes exhibit strong short-term variability, with rapid alternations between upward and downward transport. Positive nitrate events dominate overall, indicating recurrent turbulent nutrient supply toward the base of the euphotic zone. During spring tides, positive fluxes are more frequent and sustained, whereas neap-tide periods are characterized by more intermittent events and occasional strong negative excursions, particularly during the first neap period in mid-September. Thus, the spring–neap modulation is expressed primarily in the persistence and frequency of upward nutrient transport rather than in the occurrence of the largest individual flux events.

These results indicate that turbulent fluxes can generate large, episodic nutrient inputs at the base of the euphotic zone. However, the timing of the largest flux maxima appears irregular and does not strictly follow the spring–neap cycle. Instead, tidal modulation is more clearly expressed in the background pattern of nutrient supply: during spring tides, fluxes tend to be

https://doi.org/10.5194/egusphere-2026-4862
Preprint. Discussion started: 19 August 2026


smaller but more frequent and sustained, whereas during neap tides they are more sporadic and occasionally dominated by isolated extreme events. This suggests that spring tides may support a more regular turbulent nutrient input, while the strongest individual flux events remain intermittent and are likely controlled by additional physical variability such as mesoscale forcing other sources of turbulence.

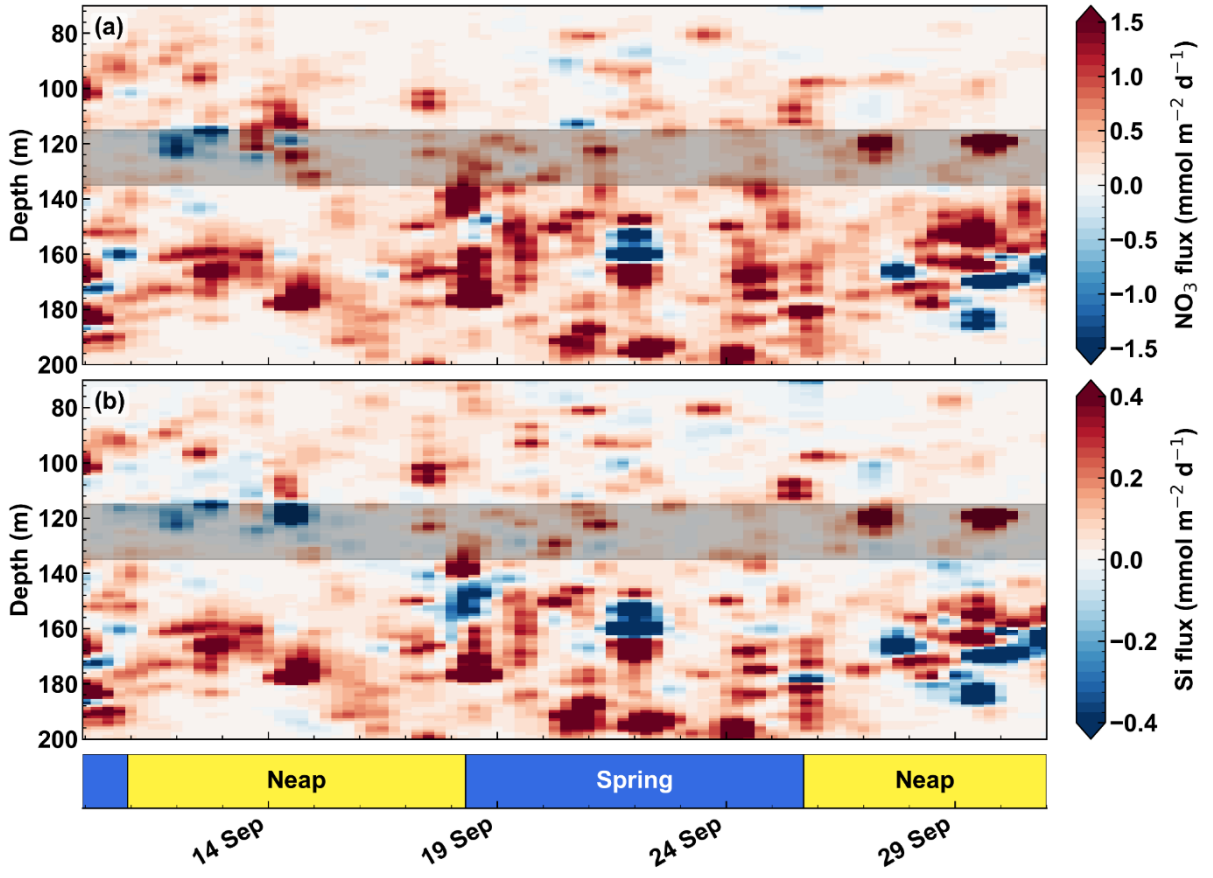

https://doi.org/10.5194/egusphere-2026-4862
Preprint. Discussion started: 19 August 2026


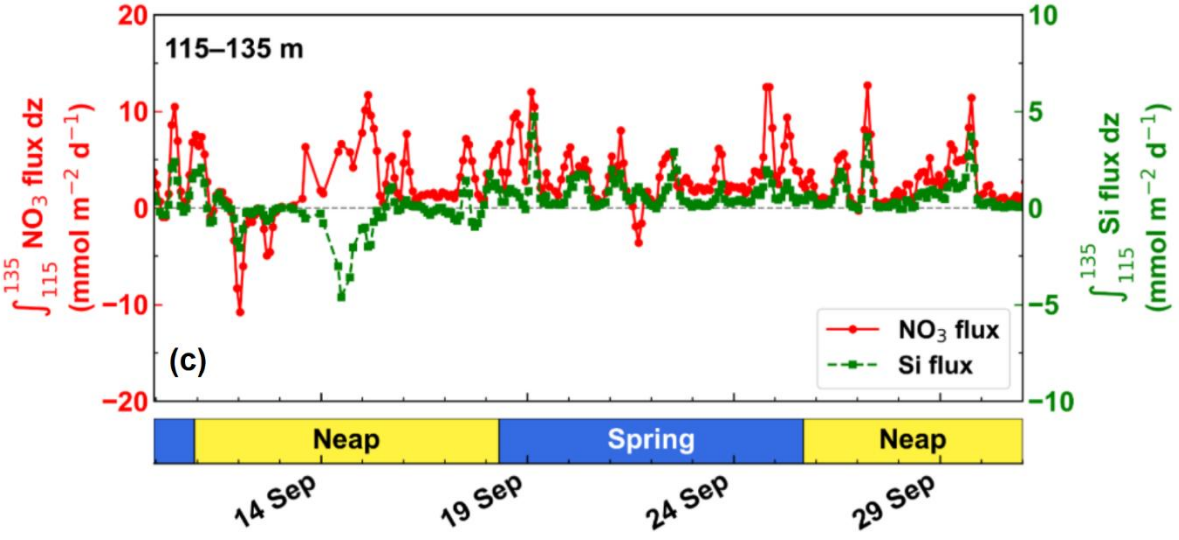


**Figure 13 : Hovmöller diagrams of turbulent nutrient fluxes between 70 and 200 m depth. Panels show the turbulent fluxes of (a) nitrate and (b) silicate, computed from glider-derived vertical diffusivity and vertical nutrient gradients. (c) Time series of turbulent nitrate and silicate fluxes integrated between 115 -135 m layer.**

Figure 14 shows the vertical structure of turbulent nutrient fluxes for $NO_3$ and Si between 70 and 200 m under spring- and neap-tide conditions. Solid lines represent the mean $F_{DIFF}$ profiles, while shaded areas indicate the interquartile range at each depth. The grey band highlights the Zeu layer, where the integrated fluxes are estimated. Overall, $NO_3$ fluxes are predominantly positive over most of the depth range, consistent with an upward turbulent nutrient supply. The spring-tide profile is generally higher than the neap-tide profile in the upper part of the section, particularly near the base of the euphotic layer. Below approximately 145 m, the neap-tide signal becomes locally more concentrated and overlaps more strongly with the spring-tide distribution. This suggests that turbulent events also occur at depth during neap tides, but affect the euphotic layer less directly. This pattern is consistent with the vertical structure observed in the dissipation profiles. At the base of the euphotic layer, turbulent nutrient fluxes remain positive under both spring- and neap-tide conditions, but the signal is stronger during spring tides. For $NO_3$, the vertically integrated flux estimated from the mean profile at Zeu is approximately 2.14 mmol $NO_3$ $m^{-2}$ $d^{-1}$ during spring tides, compared with 1.52 mmol $NO_3$ $m^{-2}$ $d^{-1}$ during neap tides. For Si, the same pattern is observed, with an integrated flux of 0.27 mmol Si $m^{-2}$ $d^{-1}$ during spring tides, compared with 0.05 mmol Si $m^{-2}$ $d^{-1}$ during neap tides.

These results indicate that turbulent nutrient fluxes are enhanced during spring tides, with a particularly strong relative increase for silicate. Overall, the observations indicate that both internal-tide-induced advection and turbulent diffusion contribute to nutrient supply at the base of the euphotic layer, although their temporal variability and relative magnitudes differ markedly

https://doi.org/10.5194/egusphere-2026-4862
Preprint. Discussion started: 19 August 2026


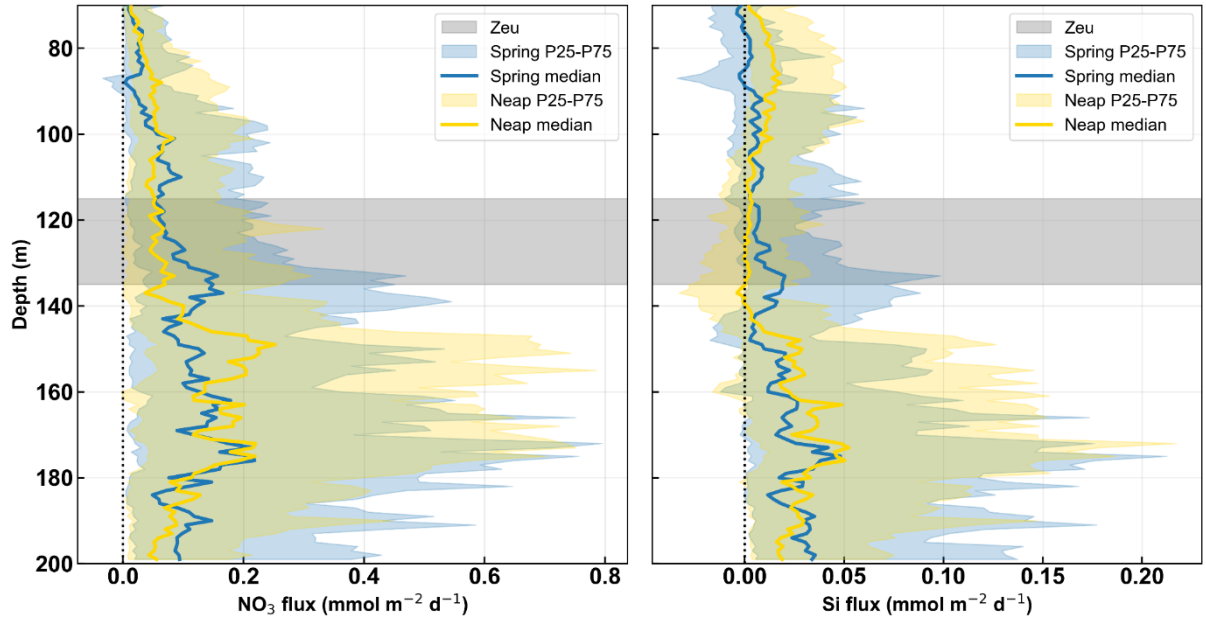


**Figure 14 : Vertical profiles of turbulent nitrate and silicate fluxes during spring and neap tidal periods between 70 and 200 m depth. Fluxes were computed from glider-derived vertical diffusivity and vertical nutrient gradients, with positive values indicating upward fluxes and negative values indicating downward fluxes. Solid lines represent mean profiles for spring (red) and neap (blue) tides events, while shaded envelopes indicate the interquartile range between the 25th and 75th percentiles. The black shaded band marks the Zeu range.**

## 4 Discussion

### 4.1 Relative Roles of Internal-Tide Advection and Turbulent Mixing in Nutrient Supply

The present results demonstrate that internal tides influence nutrient supply through two complementary but fundamentally different physical mechanisms: internal-tide-induced vertical advection redistributes existing nutrient gradients, while turbulent diffusion produces irreversible nutrient transport across density surfaces. Advection dominates the mean nutrient enrichment at the base of the euphotic layer, whereas turbulent diffusion contributes primarily through intermittent, high-intensity events. This distinction matters biogeochemically: an advective signal reflects a transient redistribution of existing

https://doi.org/10.5194/egusphere-2026-4862
Preprint. Discussion started: 19 August 2026


nutrients rather than a net input of "new" nutrients from depth, whereas turbulent fluxes constitute an irreversible supply pathway although the turbulent dissipation observed during spring tides cannot be attributed entirely to internal tides.

Following Kouogang et al. (2025), who estimated from observations at the same AMAZOMIX site that internal tides account for approximately 50% of turbulent dissipation, we applied this local scaling to isolate the internal-tide-related fraction of turbulent nutrient fluxes throughout this analysis. This should be interpreted as a first-order local estimate rather than a universal constant, since the internal-tide contribution to turbulence may vary with depth, tidal phase, and individual mixing events.

For nitrates The advective contribution is estimated at 2.3 ± 0.5 mmol $NO_3$ $m^{-2}$ $d^{-1}$, with peaks up to 10 mmol $NO_3$ $m^{-2}$ $d^{-1}$ near the base of the euphotic zone. The vertically integrated turbulent nitrate flux at Zeu reaches 2.14 mmol $NO_3$ $m^{-2}$ $d^{-1}$ during spring tides (1.52 during neap tides); restricted to the internal-tide fraction, this becomes ~1.07 mmol $NO_3$ $m^{-2}$ $d^{-1}$ roughly half the mean advective signal. However, turbulent nitrate supply is highly intermittent: total fluxes commonly reach 2–4 mmol $NO_3$ $m^{-2}$ $d^{-1}$ and can peak near 15 mmol $NO_3$ $m^{-2}$ $d^{-1}$, corresponding to internal-tide-related fluxes of 1–2 mmol $NO_3$ $m^{-2}$ $d^{-1}$ (peaks near 7 mmol $NO_3$ $m^{-2}$ $d^{-1}$) values that can exceed the mean advective estimate during episodic high-dissipation events.

For silicate The advective contribution is estimated at 0.4 ± 0.1 mmol Si $m^{-2}$ $d^{-1}$, versus a turbulent flux at Zeu of 0.27 mmol Si $m^{-2}$ $d^{-1}$ during spring tides (0.05 during neap tides), or ~0.14 mmol Si $m^{-2}$ $d^{-1}$ once restricted to the internal-tide fraction about a third of the advective contribution, indicating a stronger dominance of advective redistribution than for nitrate. Episodic turbulent fluxes nonetheless commonly reach 1–2 mmol Si $m^{-2}$ $d^{-1}$ (peaks near 5 mmol Si $m^{-2}$ $d^{-1}$), or 0.5–1 mmol Si $m^{-2}$ $d^{-1}$ (peaks near 2.5) once restricted to internal tides again exceeding the mean advective contribution during pulses.

Our field study provides the first quantitative comparison of turbulent and advective nutrient fluxes offshore of the Amazon shelf, and is consistent with prior evidence that internal tides and internal waves generate substantial nutrient fluxes across the nitracline. In European shelf seas, internal-wave-driven nitrate fluxes typically range from 1–4 mmol N $m^{-2}$ $d^{-1}$ (Sharples et al., 2001, 2007; Rippeth et al., 2009), with mean inputs of ~2 mmol $NO_3$ $m^{-2}$ $d^{-1}$ and springtime peaks near 9 mmol $NO_3$ $m^{-2}$ $d^{-1}$ at the Celtic Sea shelf edge (Sharples et al., 2009) comparable to the values reported here. Similarly strong fluxes occur in regions of intense topographic interaction, such as the Luzon Strait (~4.7 mmol $NO_3$ $m^{-2}$ $d^{-1}$; ~0.33 mmol $PO_4$ $m^{-2}$ $d^{-1}$ near a subridge; Tsutsumi et al., 2020), while other regions show more moderate but persistent fluxes: 0.07–0.44 mmol N $m^{-2}$ $d^{-1}$ (mean ~0.23) from semidiurnal pycnocline displacements (Xu et al., 2020), and ~0.45 mmol N $m^{-2}$ $d^{-1}$ (95% range 0.08–0.95) in the East China Sea (Liu et al., 2013). This regional variability reflects differences in local stratification, nutrient gradients, tidal energy, and topography.

The magnitude of the advective mechanism is consistent with typical internal-tide vertical velocities: for a semidiurnal M2 internal tide, vertical displacements of 10–100 m correspond to velocities of ~1–14 mm $s^{-1}$, sufficient to rapidly displace the nitracline or silicicline relative to the euphotic layer. The biological impact then depends on whether displaced nutrients remain within, or close enough to, the illuminated layer to be assimilated before the oscillatory motion reverses consistent

https://doi.org/10.5194/egusphere-2026-4862
Preprint. Discussion started: 19 August 2026


with Jacobsen et al. (2023), whose simulations attributed ~90% of the enhancement in primary production to internal-wave-induced advection. Our observations provide field-based support for this mechanism.

Taken together, these results show that internal tides should not be viewed solely as a mechanism enhancing turbulent mixing. Rather, they regulate nutrient availability through the combined action of reversible advective redistribution which dominates the mean nutrient budget, roughly twice the internal-tide-related turbulent flux for nitrate and three times for silicate and irreversible turbulent transport, which remains biogeochemically essential and can exceed advective inputs during short, energetic mixing events. The relative importance of each mechanism depends on the temporal and spatial scales considered.

### 4.2 Implications for ecosystems

Changes in nutrient supply do not necessarily translate into identical ecological responses, because phytoplankton groups differ in their elemental requirements. The ecological impact of internal tides therefore depends not only on the magnitude of nutrient inputs, but also on their stoichiometric composition near the base of the euphotic layer. This is particularly relevant for diatoms, which require dissolved silicate to build their frustules, whereas other groups such as cyanobacteria or small flagellates do not directly depend on silica  meaning internal-tide-driven inputs of nitrate and silicate may carry different ecological implications depending on whether they satisfy, or depart from, the requirements of silicifying organisms.

Advective nutrient anomalies were evaluated within the layer surrounding Zeu, where internal-tide-induced vertical displacements directly modulate nutrient availability. During spring tides, both nitrate and silicate exhibited positive wave-induced anomalies relative to the neutral profile, indicating net enrichment near the base of the euphotic zone: approximately 2.3 ± 0.5 mmol $NO_3$ $m^{-2}$ $d^{-1}$ for nitrate and 0.4 ± 0.1 mmol Si $m^{-2}$ $d^{-1}$ for silicate. Although both nutrients are supplied by internal-tide-driven advection, their relative supply is strongly imbalanced. The resulting advective Si:N flux ratio (≈0.4/2.3 ≈ 0.17) is much lower than the diatom Si:N uptake ratio of ~0.96 reported by Brzezinski et al. (1985), indicating that advective enrichment supplies nitrate in excess relative to silicate compared with diatom stoichiometric demand. This imbalance matters because absolute enrichment of both nutrients does not imply equally favourable conditions for all phytoplankton groups: a nitrate-rich but silicate-poor supply may broadly enhance nitrogen availability while offering comparatively little additional silicate for diatom growth. If silicate is already relatively scarce near the base of the euphotic zone  as suggested by the vertical nutrient availability indices such an input could reinforce a relative silicate constraint on diatoms despite the overall increase in nutrient availability. Internal-tide-driven advection may therefore modify not only the quantity of nutrients available near Zeu, but also the Si:N balance of the pool potentially accessible to phytoplankton.

The turbulent flux estimates show a similar stoichiometric pattern. During spring tides, the vertically integrated turbulent nitrate flux at Zeu reached ~2.14 mmol $NO_3$ $m^{-2}$ $d^{-1}$ (vs. 1.52 during neap tides), while the spring–neap contrast was stronger for silicate, rising from ~0.05 to 0.27 mmol Si $m^{-2}$ $d^{-1}$. The resulting spring-tide turbulent Si:N ratio (≈0.27/2.14 ≈ 0.13) remains well below the Brzezinski requirement, indicating that both advective and turbulent pathways supply nutrients with

https://doi.org/10.5194/egusphere-2026-4862
Preprint. Discussion started: 19 August 2026


a Si:N ratio lower than needed for balanced diatom growth. Nevertheless, turbulent mixing may still play an important ecological role: silicate shows a proportionally stronger spring-tide response than nitrate roughly a fivefold increase from neap to spring tides, versus ~40% for nitrate suggesting that intermittent turbulent events may temporarily narrow the Si:N imbalance and create short-lived windows of enhanced silicate availability. Such pulses may be particularly relevant near the deep chlorophyll maximum, where phytoplankton are exposed to both strong vertical nutrient gradients and internal-tide-driven physical variability. Studies specifically addressing silicon dynamics in internal-tide environments remain limited, but observations from tidal fronts and bank systems indicate that mixing can strongly influence silica cycling and diatom dynamics (Tweddle et al., 2013).

In the Amazon shelf region, the consistently low Si:N ratio of internal-tide-related nutrient supply suggests that internal tides may favour nitrate enrichment relative to diatom silica requirements near the base of the euphotic zone a potential stoichiometric constraint that could influence competitive interactions between silicifying and non-silicifying phytoplankton. Together with the findings of M'hamdi et al. (2025), who showed that internal tides can dilute the deep chlorophyll maximum both above and below its core, our results suggest that internal tides shape phytoplankton communities through two complementary pathways: redistributing biomass and nutrients via vertical displacements, and altering the stoichiometric balance of the nutrient supply reaching the lower euphotic layer.

## 5 Conclusion

In this study, we quantified and directly compared the relative contributions of internal-tide-driven vertical advection and turbulent diffusion to nutrient supply at the base of the euphotic layer using autonomous glider observations collected during the AMAZOMIX campaign off the Amazon shelf. The reconstructed CANYON-B nutrient fields revealed a strongly structured water column, characterized by a relative nitrate deficit in the upper layer and a relative silicate deficit at greater depth. These contrasting vertical nutrient distributions indicate distinct nutrient availability regimes above and below the base of the euphotic layer. By tracking isopycnal and nitracline vertical displacements, we showed that internal tides generate a net enrichment of nitrate and silicate near Zeu, particularly during spring tides. The estimated advective contribution reached FADV ≈ 2.3 ± 0.5 mmol $NO_3$ $m^{-2}$ $d^{-1}$ and 0.4 ± 0.1 mmol Si $m^{-2}$ $d^{-1}$. Turbulent diffusive fluxes, derived from glider-based dissipation estimates and validated against VMP measurements, also increased during spring tides. However, once the fraction attributable to internal tides was approximated as 50%, following Kouogang et al. (2025), the resulting diffusive contribution remained smaller on average, with values of approximately 1.07 mmol $NO_3$ $m^{-2}$ $d^{-1}$ and 0.14 mmol Si $m^{-2}$ $d^{-1}$.

These results demonstrate that internal-tide-driven vertical advection dominates the mean modulation of nitrate and silicate availability near the base of the euphotic layer. However, this advective contribution primarily reflects a redistribution of existing vertical nutrient gradients rather than an irreversible input of new nutrients. Turbulent diffusion, although weaker on average, remains essential because it represents a diapycnal and irreversible nutrient-supply pathway from deeper layers.

https://doi.org/10.5194/egusphere-2026-4862
Preprint. Discussion started: 19 August 2026


Moreover, turbulent diffusion can become the dominant transport mechanism during short-lived energetic mixing events, highlighting the complementary nature of these two physical processes. These findings demonstrate that the relative importance of advection and turbulent diffusion depends not only on their mean contribution but also on their temporal variability.

From an ecosystem perspective, both advective and turbulent pathways supplied nitrate in excess relative to silicate when compared with the Si:N requirements of diatoms. Beyond increasing nutrient availability, internal tides also modify the relative balance between nitrate and silicate supplied to the lower euphotic layer. Consequently, their ecological influence depends not only on the quantity of nutrients transported upward but also on their stoichiometric composition. This imbalance suggests that internal tides may enhance nutrient availability while maintaining, or even reinforcing, a relative silicate constraint near the base of the euphotic zone. Such a nitrate-rich but silicate-poor supply could potentially favour non-siliceous phytoplankton groups over diatoms, although direct community-composition observations would be required to confirm this response. A natural perspective of this work would therefore be to couple these physical observations with direct measurements of phytoplankton community composition (pigments, cytometry), in order to test whether the nutrient regime imposed by internal tides indeed favours non-siliceous groups over diatoms. Such an approach would make it possible to explicitly link the physical dynamics to the ecological structuring of phytoplankton communities at the base of the euphotic layer. Together with previous evidence for internal-tide-driven dilution of the deep chlorophyll maximum, these results suggest that internal tides off the Amazon shelf act not only as a nutrient-supply mechanism, but also as a potential structuring process for phytoplankton communities near the lower boundary of the euphotic layer. Overall, this study demonstrates that internal tides should not be regarded solely as an energetic process controlling upper-ocean mixing, but also as a key regulator of nutrient availability through the complementary action of oscillatory vertical advection and irreversible turbulent diffusion. By providing the first observational comparison of these two mechanisms off the Amazon shelf, this work offers a methodological framework that can be applied to other regions influenced by energetic internal tides. These findings highlight the importance of considering both nutrient quantity and nutrient stoichiometry when assessing the role of internal tides in shaping biogeochemical processes and ecosystem functioning in stratified tropical oceans.

## Code and data availability

The AMAZOMIX glider dataset is publicly available at SEANOE (https://doi.org/10.17882/108213, M'hamdi et al., 2025)..

https://doi.org/10.5194/egusphere-2026-4862
Preprint. Discussion started: 19 August 2026


## Author contributions

AKL: funding acquisition. AM : conceptualization and methodology. AM, with assistance from AB: data pre-processing. Formal analysis: AM with interactions from all co-authors. Preparation of the article: AM with contributions from all co-authors.

## Competing interests

The contact author has declared that none of the authors has any competing interests.

## Acknowledgements

Alex Costa da Silva acknowledge the support of the Brazilian funding agency CNPq (National Council for Scientific and Technological Development). The authors would like to thank the "Flotte Océanographique Française" and the officers and crew of the R/V Antea for their contribution to the success of the operations aboard as well as all the scientists involved in data and water sample collection for their valuable support during and after the AMAZOMIX cruise. We acknowledge the Brazilian authorities for authorizing the survey, the French National Park of Instrumentation (DT-INSU) for their instrument during the cruise and support in data analysis, and USIMAGO from IRD for their help during the cruise and for biogeochemical data analysis. This work is a contribution to the LMI TAPIOCA (https://www.tapioca.ird.fr, last access: 12 August 2026).

## Financial support

This work is a part of the project "AMAZOMIX", funded by multiple agencies: the "Flotte Océanographique Française" that funded the 40d at sea of the R/V Antea, the Institut de Recherche pour le Développement (IRD), via among others, LMI TAPIOCA, CNES, within the framework of the APR TOSCA MIAMAZ TOSCA project (PIs Ariane Koch-Larrouy, Vincent Vantrepotte, and Isabelle Dadou), the LEGOS, and the program international Franco-Brazileiro GUYAMAZON(callno.005/2017). It is also part of the PhD thesis of Amine M'hamdi, funded by the Fundação de Amparo a Ciência e Tecnologia do Estado de Pernambuco (FACEPE) (IBPG-10781.08/22), under the co-advisement of Ariane Koch-Larrouy, Alex Costa da Silva, Isabelle Dadou, and Vincent Vantrepotte.

https://doi.org/10.5194/egusphere-2026-4862
Preprint. Discussion started: 19 August 2026


**Review statement**

The review statement will be added by Copernicus Publications listing the handling editor as well as all contributing referees according to their status anonymous or identified.

**References**

690 Althaus, A. M., Kunze, E., and Sanford, T. B.: Internal tide radiation from Mendocino Escarpment, J. Phys. Oceanogr., 33, 1510–1527, https://doi.org/10.1175/1520-0485(2003)033%3C1510:ITRFME%3E2.0.CO;2, 2003.

Assene, F., Koch-Larrouy, A., Dadou, I., Tchilibou, M., Morvan, G., Chanut, J., Costa da Silva, A., Vantrepotte, V., Allain, D., and Tran, T.-K.: Internal tides off the Amazon shelf – Part 1: The importance of the structuring of ocean temperature during two contrasted seasons, Ocean Sci., 20, 43–67, https://doi.org/10.5194/os-20-43-2024, 2024.

695 Baines, P. G.: On internal tide generation models, Deep Sea Res. Part Oceanogr. Res. Pap., 29, 307–338, https://doi.org/10.1016/0198-0149(82)90098-X, 1982.

Beaird, N., Fer, I., Rhines, P., and Eriksen, C.: Dissipation of Turbulent Kinetic Energy Inferred from Seagliders: An Application to the Eastern Nordic Seas Overflows, J. Phys. Oceanogr., 42, 2268–2282, https://doi.org/10.1175/JPO-D-12-094.1, 2012.

700 Bittig, H. C., Steinhoff, T., Claustre, H., Fiedler, B., Williams, N. L., Sauzède, R., Körtzinger, A., and Gattuso, J.-P.: An alternative to static climatologies: Robust estimation of open ocean CO2 variables and nutrient concentrations from T, S, and O2 data using Bayesian neural networks, Front. Mar. Sci., 5, 328, https://doi.org/10.3389/fmars.2018.00328, 2018.

Bourgault, D., Hamel, C., Cyr, F., Tremblay, J.-É., Galbraith, P. S., Dumont, D., and Gratton, Y.: Turbulent nitrate fluxes in the Amundsen Gulf during ice-covered conditions, Geophys. Res. Lett., 38, L15602, https://doi.org/10.1029/2011GL047936, 705 2011.

Brandt, P., Rubino, A., and Fischer, J.: Large-Amplitude Internal Solitary Waves in the North Equatorial Countercurrent, J. Phys. Oceanogr., 32, 1567–1573, https://doi.org/10.1175/1520-0485(2002)032%3C1567:LAISWI%3E2.0.CO;2, 2002.

Brzezinski, M. A.: THE Si:C:N RATIO OF MARINE DIATOMS: INTERSPECIFIC VARIABILITY AND THE EFFECT OF SOME ENVIRONMENTAL VARIABLES, J. Phycol., 21, 347–357, https://doi.org/10.1111/j.0022-3646.1985.00347.x, 710 1985.

Capuano, T. A., Koch-Larrouy, A., Nugroho, D., Zaron, E., Dadou, I., Tran, K., Vantrepotte, V., and Allain, D.: Impact of Internal Tides on Distributions and Variability of Chlorophyll-a and Nutrients in the Indonesian Seas, J. Geophys. Res. Oceans, 130, e2022JC019128, https://doi.org/10.1029/2022JC019128, 2025.

De Macedo, C. R., Koch-Larrouy, A., da Silva, J. C. B., Magalhães, J. M., Lentini, C. A. D., Tran, T. K., Rosa, M. C. B., and 715 Vantrepotte, V.: Spatial and temporal variability in mode-1 and mode-2 internal solitary waves from MODIS-Terra sun glint off the Amazon shelf, Ocean Sci., 19, 1357–1374, https://doi.org/10.5194/os-19-1357-2023, 2023.

https://doi.org/10.5194/egusphere-2026-4862
Preprint. Discussion started: 19 August 2026


De Macedo, C. R., Koch-Larrouy, A., da Silva, J. C. B., Magalhães, J. M., Assene, F., Tran, M. D., Dadou, I., M'Hamdi, A., Tran, T. K., and Vantrepotte, V.: Tidal signatures on surface chlorophyll a concentration in the Brazilian Equatorial Margin, Ocean Sci., 22, 871–892, https://doi.org/10.5194/os-22-871-2026, 2026.

Evans, D. G., Lucas, N. S., Hemsley, V. S., Frajka-Williams, E., Naveira Garabato, A. C., Martin, A. P., Painter, S. C., Inall, M. E., and Palmer, M. R.: Annual Cycle of Turbulent Dissipation Estimated from Seagliders, Geophys. Res. Lett., 45, 10560–10569, https://doi.org/10.1029/2018GL079966, 2018.

Evans, M. A., MacIntyre, S., and Kling, G. W.: Internal wave effects on photosynthesis: Experiments, theory, and modeling, Limnol. Oceanogr., 53, 339–353, https://doi.org/10.4319/lo.2008.53.1.0339, 2008.

Garau, B., Ruiz, S., Zhang, W. G., Pascual, A., Heslop, E., Kerfoot, J., and Tintoré, J.: Thermal Lag Correction on Slocum CTD Glider Data, J. Atmos. Ocean. Technol., 28, 1065–1071, https://doi.org/10.1175/JTECH-D-10-05030.1, 2011.

Garrett, C. and Kunze, E.: Internal Tide Generation in the Deep Ocean, Annu. Rev. Fluid Mech., 39, 57–87, https://doi.org/10.1146/annurev.fluid.39.050905.110227, 2007.

Garwood, J. C., Musgrave, R. C., and Lucas, A. J.: Life in internal waves, Oceanography, 33, 38–49, https://doi.org/10.5670/oceanog.2020.313, 2020.

Goret, C., Koch-Larrouy, A., Kouogang, F., de Macedo, C. R., M'Hamdi, A., Magalhães, J. M., da Silva, J. C. B., Tchilibou, M., Artana, C., Dadou, I., Delepoulle, A., Barbot, S., Ballarotta, M., Carrère, L., and Costa da Silva, A.: Internal solitary waves refraction and diffraction from interaction with eddies off the Amazon Shelf from SWOT, Ocean Sci., 22, 679–698, https://doi.org/10.5194/os-22-679-2026, 2026.

Holloway, G. and Denman, K.: Influence of internal waves on primary production, J. Plankton Res., 11, 409–413, https://doi.org/10.1093/plankt/11.2.409, 1989.

Ivanov, V. A., Ivanov, L. I., and Lisichenok, A. D.: Redistribution of energy of the internal tidal wave in the North Equatorial Countercurrent region, Sov. J. Phys. Oceanogr., 1, 383–386, https://doi.org/10.1007/BF02196837, 1990.

Jacobsen, J. R., Edwards, C. A., Powell, B. S., Colosi, J. A., and Fiechter, J.: Nutricline adjustment by internal tidal beam generation enhances primary production in idealized numerical models, Front. Mar. Sci., 10, 1309011, https://doi.org/10.3389/fmars.2023.1309011, 2023.

Jensen, J. L. W. V.: Sur les fonctions convexes et les inégalités entre les valeurs moyennes, Acta Math., 30, 175–193, https://doi.org/10.1007/BF02418571, 1906.

Koch-Larrouy, A., Lengaigne, M., Terray, P., Madec, G., and Masson, S.: Tidal mixing in the Indonesian Seas and its effect on the tropical climate system, Clim. Dyn., 34, 891–904, https://doi.org/10.1007/s00382-009-0642-4, 2010.

Kouogang, F., Koch-Larrouy, A., Magalhaes, J., Costa da Silva, A., Kerhervé, D., Bertrand, A., Cervelli, E., Assene, F., Ternon, J.-F., and Rousselot, P.: Turbulent dissipation along contrasting internal tide paths off the Amazon shelf from AMAZOMIX, Ocean Sci., 21, 1589–1608, https://doi.org/10.5194/os-21-1589-2025, 2025.

https://doi.org/10.5194/egusphere-2026-4862
Preprint. Discussion started: 19 August 2026


Kouogang, F., Koch-Larrouy, A., Carton, X., Assene, F., Morvan, G., and Araujo, M.: Internal tides–cyclonic eddy interaction and intermodal energy pathways: evidence from 3 km NEMO-AMAZON36 simulations, Ocean Sci., 22, 1545–1568, https://doi.org/10.5194/os-22-1545-2026, 2026.

Krahmann, G.: GEOMAR FB1-PO Matlab Slocum glider processing toolbox, GEOMAR Helmholtz Centre for Ocean Research Kiel, https://doi.org/10.3289/SW_4_2023, 2023.

Kunze, E.: Internal-Wave-Driven Mixing: Global Geography and Budgets, J. Phys. Oceanogr., 47, 1325–1345, https://doi.org/10.1175/JPO-D-16-0141.1, 2017.

Lande, R. and Yentsch, C. S.: Internal waves, primary production and the compensation depth of marine phytoplankton, J. Plankton Res., 10, 565–571, https://doi.org/10.1093/plankt/10.3.565, 1988.

Li, Q. P., Zhou, W., Chen, Y., and Wu, Z.: Phytoplankton response to a plume front in the northern South China Sea, Biogeosciences, 15, 2551–2563, https://doi.org/10.5194/bg-15-2551-2018, 2018.

Lucas, A. J., Franks, P. J. S., and Dupont, C. L.: Horizontal internal-tide fluxes support elevated phytoplankton productivity over the inner continental shelf, Limnol. Oceanogr. Fluids Environ., 1, 56–74, https://doi.org/10.1215/21573698-1258185, 2011.

Lyard, F. H., Allain, D. J., Cancet, M., Carrère, L., and Picot, N.: FES2014 global ocean tide atlas: design and performance, Ocean Sci., 17, 615–649, https://doi.org/10.5194/os-17-615-2021, 2021.

Ma, L., Bai, X., Laws, E. A., Xiao, W., Guo, C., Liu, X., Chiang, K., Gao, K., and Huang, B.: Responses of Phytoplankton Communities to Internal Waves in Oligotrophic Oceans, J. Geophys. Res. Oceans, 128, e2023JC020201, https://doi.org/10.1029/2023JC020201, 2023.

Magalhaes, J. M., da Silva, J. C. B., Buijsman, M. C., and Garcia, C. A. E.: Effect of the North Equatorial Counter Current on the generation and propagation of internal solitary waves off the Amazon shelf (SAR observations), Ocean Sci., 12, 243–255, https://doi.org/10.5194/os-12-243-2016, 2016.

M'hamdi, A., Koch-Larrouy, A., Costa da Silva, A., Dadou, I., de Macedo, C. R., Bosse, A., Vantrepotte, V., Aguedjou, H. M., Tran, T.-K., Testor, P., Mortier, L., Bertrand, A., Mendes de Castro Melo, P. A., Lee, J., Rollnic, M., and Araujo, M.: Impact of internal tides on chlorophyll a distribution and primary production off the Amazon shelf from glider measurements and satellite observations, Ocean Sci., 21, 2873–2894, https://doi.org/10.5194/os-21-2873-2025, 2025.

M'hamdi Amine, Bosse Anthony, Testor Pierre, Mortier Laurent, Rousselot Pierre, Costa da Silva Alex, Araujo Moacyr, Koch-Larrouy Ariane, Bertrand Arnaud (2025). AMAZOMIX cruise - Glider dataset. SEANOE. https://doi.org/10.17882/108213

Moore, J. K., Lindsay, K., Doney, S. C., Long, M. C., and Misumi, K.: Marine ecosystem dynamics and biogeochemical cycling in the Community Earth System Model [CESM1(BGC)]: Comparison of the 1990s with the 2090s under the RCP4.5 and RCP8.5 scenarios, J. Clim., 26, 9291–9312, https://doi.org/10.1175/JCLI-D-12-00566.1, 2013.

Osborn, T. R.: Estimates of the local rate of vertical diffusion from dissipation measurements, J. Phys. Oceanogr., 10, 83–89, https://doi.org/10.1175/1520-0485(1980)010%3C0083:EOTLRO%3E2.0.CO;2, 1980.

https://doi.org/10.5194/egusphere-2026-4862
Preprint. Discussion started: 19 August 2026


Ray, R. D. and Susanto, R. D.: Tidal mixing signatures in the Indonesian seas from high-resolution sea surface temperature data, Geophys. Res. Lett., 43, 8115–8123, https://doi.org/10.1002/2016GL069485, 2016.

Sharples, J., Tweddle, J. F., Green, J. A. M., Palmer, M. R., Kim, Y.-N., Hickman, A. E., Holligan, P. M., Moore, C. M., Rippeth, T. P., Simpson, J. H., and Krivtsov, V.: Spring-neap modulation of internal tide mixing and vertical nitrate fluxes at a shelf edge in summer, Limnol. Oceanogr., 52, 1735–1747, https://doi.org/10.4319/lo.2007.52.5.1735, 2007.

Sharples, J., Moore, C. M., Hickman, A. E., Holligan, P. M., Tweddle, J. F., Palmer, M. R., and Simpson, J. H.: Internal tidal mixing as a control on continental margin ecosystems, Geophys. Res. Lett., 36, L23603, https://doi.org/10.1029/2009GL040683, 2009.

Tchilibou, M., Koch-Larrouy, A., Barbot, S., Lyard, F., Morel, Y., Jouanno, J., and Morrow, R.: Internal tides off the Amazon shelf during two contrasted seasons: interactions with background circulation and SSH imprints, Ocean Sci., 18, 1591–1618, https://doi.org/10.5194/os-18-1591-2022, 2022.

Tuerena, R. E., Williams, R. G., Mahaffey, C., Vic, C., Green, J. A. M., Naveira-Garabato, A., Forryan, A., and Sharples, J.: Internal Tides Drive Nutrient Fluxes Into the Deep Chlorophyll Maximum Over Mid-ocean Ridges, Glob. Biogeochem. Cycles, 33, 995–1009, https://doi.org/10.1029/2019GB006214, 2019.

Villamaña, M., Mouriño-Carballido, B., Marañón, E., Cermeño, P., Chouciño, P., da Silva, J. C. B., Díaz, P. A., Fernández-Castro, B., Gilcoto, M., Graña, R., Latasa, M., Magalhaes, J. M., Otero-Ferrer, J. L., Reguera, B., and Scharek, R.: Role of internal waves on mixing, nutrient supply and phytoplankton community structure during spring and neap tides in the upwelling ecosystem of Ría de Vigo (NW Iberian Peninsula), Limnol. Oceanogr., 62, 1014–1030, https://doi.org/10.1002/lno.10482, 2017.

Vlasenko, V., Stashchuk, N., and Hutter, K.: Baroclinic Tides: Theoretical Modeling and Observational Evidence, Cambridge University Press, https://doi.org/10.1017/CBO9780511535932, 2005.

Waterhouse, A. F., MacKinnon, J. A., Nash, J. D., Alford, M. H., Kunze, E., Simmons, H. L., Polzin, K. L., St. Laurent, L. C., Sun, O. M., and Pinkel, R.: Global patterns of diapycnal mixing from measurements of the turbulent dissipation rate, J. Phys. Oceanogr., 44, 1854–1872, https://doi.org/10.1175/JPO-D-13-0104.1, 2014.